Large seasonal and interannual variations of biogenic sulfur compounds in the Arctic atmosphere (Svalbard; 78.9° N, 11.9° E)

Sehyun Jang[1,*], Ki-Tae Park[2,3,*], Kitack Lee[1,4], Young Jun Yoon[2], Kitae Kim[2,3],
Hyun Young Chung[2,3], Eunho Jang[2,3], Silvia Becagli[5], Bang Yong Lee[2], Rita Traversi[5],
Konstantinos Eleftheriadis[6], Radovan Krejci[7], Ove Hermansen[8]

[1]Division of Environmental Science and Engineering, Pohang University of Science and Technology, Pohang, 37673, Korea
[2]Korea Polar Research Institute (KOPRI), 26 Songdomirae-ro, Yeonsu-gu, Incheon, 21990, Korea
[3]University of Science and Technology, Daejeon, 34113, Korea
[4]Institute for Convergence Research and Education in Advanced Technology, Yonsei University, Seoul, 03722, Korea
[5]Institute of Polar Science, ISP-CNR, via Torino, 155, Venezia Mestre, (VE) 30172, Italy
[6]N.C.S.R. "Demokritos", Environmental Radioactivity Laboratory, Ag. Paraskevi, 15341, Attiki, Greece
[7]Department of Environmental Science and Analytical Chemistry & Bolin Centre for Climate Research, Stockholm University, Stockholm 10691, Sweden
[8]Norwegian Institute for Air Research, Kjeller, Norway

*These authors contributed equally to this work.

Correspondence to: Kitack Lee (ktl@postech.ac.kr) and Young Jun Yoon (yjyoon@kopri.re.kr)

Abstract. Seasonal to interannual variations in the concentrations of sulfur aerosols (< 2.5 μm in diameter; non sea-salt sulfate: NSS-SO$_4^{2-}$; anthropogenic sulfate: Anth-SO$_4^{2-}$; biogenic sulfate: Bio-SO$_4^{2-}$; methanesulfonic acid: MSA) in the Arctic atmosphere were investigated using measurements of the chemical composition of aerosols collected at Ny-Ålesund, Svalbard (78.9° N, 11.9° E) from 2015 to 2019. In all measurement years the concentration of NSS-SO$_4^{2-}$ was highest during the pre-bloom period and rapidly decreased towards summer. During the pre-bloom period we found a strong correlation between NSS-SO$_4^{2-}$ (sum of Anth-SO$_4^{2-}$ and Bio-SO$_4^{2-}$) and Anth-SO$_4^{2-}$. This was because more than 50 % of the NSS-SO$_4^{2-}$ measured during this period was Anth-SO$_4^{2-}$, which originated in the northern Europe and was subsequently transported to the Arctic in Arctic haze. Unexpected increases in the concentration of Bio-SO$_4^{2-}$ aerosols (an oxidation product of dimethylsulfide: DMS) were occasionally found during the pre-bloom period. These probably originated in regions to the south (the North Atlantic Ocean and the Norwegian Sea), rather than in ocean areas in the proximity of Ny-Ålesund. Another oxidation product of DMS is MSA, and the ratio of MSA to Bio-SO$_4^{2-}$ is extensively used to estimate the total amount of DMS-derived aerosol particles in remote marine environments. The concentration of MSA during the pre-bloom period remained low, primarily because of the greater loss of MSA relative to Bio-SO$_4^{2-}$, and the suppression of condensation of gaseous MSA onto particles already present in air masses being transported northwards from distant ocean source regions (existing particles). In addition, the low light intensity during the pre-bloom period resulted in a low concentration of photochemically activated oxidant species including OH radicals and BrO; these conditions favored the

35 oxidation pathway of DMS to Bio-SO_4^{2-} rather than to MSA, which acted to lower the MSA concentration at Ny-Ålesund. The concentration of MSA peaked in May or June, and was positively correlated with phytoplankton biomass in the Greenland and Barents seas around Svalbard. As a result, the mean ratio of MSA to the DMS-derived aerosols was low (0.09 ± 0.07) in the pre-bloom period, but high (0.32 ± 0.15) in the bloom and post-bloom periods. There was large interannual variability in the ratio of MSA to Bio-SO_4^{2-} (i.e., 0.24 ± 0.11 in 2017, 0.40 ± 0.14 in 2018, and 0.36 ± 0.14 in 2019) during

40 the bloom and post-bloom periods. This was probably associated with changes in the chemical properties of existing particles, biological activities surrounding the observation site, and air mass transport patterns. Our results indicate that MSA is not a conservative tracer for predicting DMS-derived particles, and the contribution of MSA to the growth of newly formed particles may be much larger during the bloom and post-bloom periods than during the pre-bloom period.

1. Introduction

45   Aerosols alter the radiative properties of the Earth's surface by means of direct (e.g., scattering and absorption of solar radiation) and indirect (e.g., cloud life-time) effects, and thereby contribute to climate change (Albrecht, 1989; Haywood and Boucher, 2000; Sekiguchi et al., 2003). Moreover, acidification of the Arctic Ocean has been enhanced because of the increasing addition of anthropogenic CO_2, facilitated by ocean freshening and greater air-sea CO_2 exchange (Lee et al., 2011); and ocean acidification potentially impacts on the net production and fluxes of marine trace gases, and so

50 affects climate (Hoppkins et al., 2020). The recent acceleration of Arctic warming has highlighted the role of natural aerosols in influencing the radiative properties of the Arctic atmosphere (Dall'Osto et al., 2017; Willis et al., 2018). Nonetheless, current knowledge of the effect of aerosols on climate regulation and the mechanisms of formation of natural aerosols is far from comprehensive, and more alarmingly is ambiguous (Mahowald et al., 2011; IPCC, 2013). Sulfurous compounds including SO_2, methanesulfonic acid, and hydroperoxymethyl thioformate in the atmosphere are the oxidation products of

55 dimethyl sulfide (DMS). These effectively form new particles through homogeneous nucleation and clustering reactions that are closely linked to water vapor and ammonia (negative ion-induced ternary nucleation), and contribute to particle growth (Kulmala, 2003; Kulmala et al., 2004; Veres et al., 2020). Sulfuric acid is widely recognized as a driver of new particle formation (NPF) (Kulmala, 2003), whereas methanesulfonic acid (MSA) particles tend to condense onto particles that are already present (existing particles), and so contribute to particle growth (Wyslouzil, et al., 1991; Leaitch et al., 2013;

60 Hayashida et al., 2017). However, recent studies have provided evidence for MSA involvement in new particle formation; for example, the reaction of MSA with amines or ammonia in the presence of water results in particle formation and growth (Dawson et al., 2012; Chen et al., 2015; 2016a). MSA also indirectly contributes to NPF by enhancing the formation of H_2SO_4-amines clusters (Bork et al., 2014). Some studies have reported that MSA only increased the mass of particles and not their number (Hoffmann et al., 2016; Yan et al., 2020), suggesting a minor role for MSA in NPF. The growth of particles

65 following NPF is particularly crucial in generating cloud condensation nuclei (CCN), which eventually lead to cloud formation. As a result, naturally produced gas molecules can promote NPF and subsequent growth of particles in the

presence of sulfate and MSA (DMS oxidation products) (Chang et al., 2011a; Burkart et al., 2017). Hence, data on the quantities of non sea-salt sulfate (NSS-SO$_4^{2-}$) and MSA and their variations are crucial in elucidating NPF and particle growth, and ultimately the role of ocean phytoplankton in modulation of the radiative properties of the Arctic atmosphere.

70   The origins of sulfate aerosols include sea-salt sulfate (ss-SO$_4^{2-}$), anthropogenic SO$_2$, volcanic SO$_2$, boreal production of natural precursor, and DMS (Bates et al., 1992a). Among those, DMS is produced through multiple biological processes occurring in pelagic and sympagic ecosystems (e.g., Kettle and Andreae, 2000; Stefels et al., 2007; Kim et al., 2010; Lee et al., 2012; Levasseur, 2013; Park et al., 2014a; Park et al. 2019). Some of the DMS is ultimately released into the atmosphere through air-sea gas exchange processes. Airborne DMS is rapidly oxidized to SO$_2$ via hydrogen abstraction

75   by OH radicals, nitrate, and chlorine; to hydroperoxymethyl thioformate via hydrogen shift by OH radicals; and to MSA via OH addition by OH radicals and in part by halogen oxides (von Glasow and Crutzen, 2004; Barnes et al., 2006; Veres et al., 2020). Seasonal variations in the product ratio of DMS oxidized to MSA and biogenic sulfate (Bio-SO$_4^{2-}$) over the Arctic region reflect the complexity of aerosol chemistry. The product ratio of DMS oxidation is highly variable, and is affected by air temperature, relative humidity, precipitation, and solar radiation (Hynes et al., 1986; Yin et al., 1990; Bates et al., 1992b).

80   Among those factors involved, air temperature is known to largely determine the oxidation pathways of DMS. At ambient temperatures the proportions of MSA and Bio-SO$_4^{2-}$ are typically 0.25 and 0.75, respectively (Hynes et al., 1986). DMS is well known to be oxidized more to MSA at lower temperatures. The observed latitudinal variations in the product ratio of DMS oxidation are largely consistent with those predicted from the temperature dependence of the oxidation pathway of DMS (Hynes et al., 1986; Berresheim et al., 1990; Bates et al., 1992b), although equally available are reports on an absence

85   of temperature dependence (Ayers et al., 1991; Prospero et al., 1991; Chen et al., 2012). The product ratio of DMS oxidation is a result of the net effect of multiple processes, including concentration of atmospheric oxidants and meteorological factors influencing DMS oxidation. Therefore, the ratio could vary considerably among seasons and years.

     To investigate DMS oxidation pathways in the Arctic atmosphere we measured sulfate aerosol concentrations at 3-day intervals from 2015 to 2019; this provided comprehensive datasets encompassing seasonal and interannual variations in

90   sulfate and MSA concentrations in aerosol particles in the Arctic atmosphere. In particular, S isotope ratios were measured for all aerosol samples, and were used to partition the total NSS-SO$_4^{2-}$ into anthropogenic sulfate (Anth-SO$_4^{2-}$) and Bio-SO$_4^{2-}$ (the oxidative product of biogenic DMS). We also calculated the product ratio of MSA to biogenic-S-aerosols (MSA + Bio-SO$_4^{2-}$: Bio-S-aerosol). Analysis of Anth-SO$_4^{2-}$, Bio-SO$_4^{2-}$, and MSA concentration data, in conjunction with data on air mass back-trajectories enabled identification of the sources of S aerosols, and elucidation of factors governing variations in

95   their concentrations.

2. Materials and methods

2.1. Sampling site and aerosol sampling

Aerosol samples were collected at 50 m above sea level at the Gruvebadet observatory (78.9° N, 11.9° E; Fig. 1a) at Ny-Ålesund, Svalbard. Sampling covered the phytoplankton pre-bloom (defined as March to the 2nd week of April), bloom (3rd week of April to the 2nd week of June), and post-bloom periods (3rd week of June onwards). Division of these periods was subjectively made based on the mean chlorophyll-*a* (Chl-*a*) concentration in the Greenland and Barents seas near Svalbard. The period during which the concentration of Chl-*a* was > 0.5 mg m^{-3} was defined as the phytoplankton bloom period, whereas the periods when the concentration of Chl-*a* was < 0.5 mg m^{-3} prior to and following the bloom were defined as the pre-bloom and post-bloom periods, respectively.

Aerosol samples were collected at 3-day intervals using a high volume sampler (HV-1000R; SIBATA, Japan) outfitted with a PM 2.5 impactor (collecting particles < 2.5 µm in aerodynamic equivalent diameter). The aerosol sampler was mounted on the roof of the Gruvebadet observatory. Particulate matter in the atmosphere was collected on a quartz filter over approximately 72 h at a flow rate of 1000 L min^{-1}, corresponding to a total air volume of 4320 m^3. The method of aerosol sampling has been described elsewhere (Park et al., 2017).

2.2. Atmospheric DMS mixing ratio and major ions in aerosol samples

The analytical system enabling measurement of atmospheric DMS mixing ratio at parts per trillion levels is equipped with a DMS trapping component, a gas chromatograph, and a pulsed flame photometric detector. The detection limit of the DMS system was close to 1.5 pptv with a sampling air volume of 6 L and the description of the system can be found elsewhere (Jang et al., 2016).

For determination of concentrations of major ions, a disk filter (47-mm diameter) was taken from a whole quartz filter (20.3 cm × 25.4 cm), soaked in 50 mL of Milli-Q water and sonicated in a bath for 60 min; aliquots of this solution were used for analysis. Milli-Q water used for the ion extraction was produced using a water purification system (Milli-Q Direct 16, Merck Millipore, USA). The concentrations of water-extractable inorganic anions and cations including MSA, were measured using ion chromatography (Dionex ICS-1100, Thermo Fisher Scientific Inc., USA) fitted with an IonPac AS 19 column (Thermo Fisher Scientific Inc., USA). The instrumental detection limits were 0.02 µg L^{-1} for MSA and 0.02 µg L^{-1} for SO_4^{2-}. From replicate injections, the analytical precision was determined to be < 5 % (relative standard deviation).

2.3. Stable S isotope ratio in sulfate aerosols

For measurement of stable S isotope ratio ($\delta^{34}S$) in an aerosol sample, half of the quartz filter was soaked in 50 mL Milli-Q water and sonicated for 60 min. Then, 50–100 µL of 1 M HCl was added to the solution (resulting in a pH of 3–4),

125 after which 100 µL of 1 M BaCl$_2$ solution was injected into the solution, leading to gradual precipitation of BaSO$_4$. Following the completion of precipitation over 24 h, the BaSO$_4$ precipitates were filtered onto a membrane filter and dried for another 24 h prior to S isotope ratio measurement. Each membrane filter was packed into a tin capsule and analyzed using an isotope ratio mass spectrometer (IsoPrime100; IsoPrime Ltd, UK) and an elemental analyzer (Vario MICRO cube; Elementar Co., Germany). Each filter treatment was carried out in a laminar flow hood to minimize contamination.

130 International standard reference materials were used to measure the abundance of S isotope in the aerosols. We used NBS-127 (20.3 ± 0.4 ‰), IAEA-S1 (silver sulfide; -0.3 ± 0.3 ‰), and IAEA-S2 (silver sulfide; 22.7 ± 0.2 ‰) (Coplen and Krouse, 1998; Halas and Szaran, 2001; Santamaria-Fernandez et al., 2008) to prepare the calibration curve. NBS-127 was used as the primary standard reference material, and was measured with every five samples.

The resulting S isotope ratio of an aerosol sample (δ^{34}S) was expressed (Eq. 1) as parts per thousand (‰) relative to 135 the ^{34}S/^{32}S ratio of a standard (Vienna-Canyon Diablo Troilite) (Krouse and Grinenko, 1991).

$$\delta^{34}S\ (‰) = \{(^{34}S/^{32}S)_{sample}/(^{34}S/^{32}S)_{standard} - 1\} \times 1000 \tag{1}$$

Among known sources, both Anth-SO$_4^{2-}$ and Bio-SO$_4^{2-}$ are the main sources of sulfate aerosols in the Arctic environment 140 (Udisti et al., 2016; Park et al., 2017). Data on the S isotope ratio of aerosol particles and the concentrations of major ions enabled estimation of the contributions of biogenic DMS (f_{bio}), anthropogenic SO$_x$ (f_{anth}), and ss-SO$_4^{2-}$ (f_{ss}) to the total SO$_4^{2-}$ concentration. The concentration of ss-SO$_4^{2-}$ was estimated using the seawater ratio of SO$_4^{2-}$ to Na$^+$ (0.252; Keene et al., 1986). The NSS-SO$_4^{2-}$ fraction of the total SO$_4^{2-}$ was then calculated by subtracting the fraction of ss-SO$_4^{2-}$ from the total SO$_4^{2-}$. The fraction of biogenic SO$_4^{2-}$ was estimated by solving the following equations:

145

$$f_{anth} + f_{bio} + f_{ss} = 1 \tag{2}$$

$$\delta^{34}S_{sample} = f_{anth}\delta^{34}S_{anth} + f_{bio}\delta^{34}S_{bio} + f_{ss}\delta^{34}S_{ss} \tag{3}$$

$$f_{ss} = [SO_4^{2-}/Na^+]_{ss} \cdot [Na^+/SO_4^{2-}]_{sample} \tag{4}$$

150 To solve equations 2–4 we used the reported S isotope ratios (δ^{34}S) of ss-SO$_4^{2-}$ (21.0 ± 0.1 ‰), Anth-SO$_4^{2-}$ (5 ± 1 ‰), and Bio-SO$_4^{2-}$ (18 ± 2 ‰) (Norman et al., 1999; Böttcher et al., 2007; Lin et al., 2012). Based on measurements of the S isotope ratio on aerosol samples, then we calculated the fraction of MSA (R_{Bio} = MSA / [MSA + Bio-SO$_4^{2-}$]) in the total biogenic-S-aerosols to evaluate the oxidative pathway of DMS to MSA or to Bio-SO$_4^{2-}$. In calculating R_{Bio}, some data (~23 data) having low Bio-SO$_4^{2-}$ values (< 25 ng m^{-3}) were not included because unusually low Bio-SO$_4^{2-}$ values resulted in biases in the R_{Bio} 155 values (Table S1).

2.4. Black carbon

An aethalometer (model AE31; Magee Scientific Co., USA) installed at the Zeppelin station was used to analyze the concentration of equivalent black carbon by measuring light-absorbing particles at a wavelength of 880 nm, as described by Eleftheriadis et al. (2009). The good congruence between the concentrations of Anth-SO_4^{2-} and black carbon measured during the pre-bloom period (March to April) indicates that variations in black carbon were reasonably consistent with variations in Anth-SO_4^{2-}, reflecting that both Anth-SO_4^{2-} and black carbon had common sources (i.e., fossil fuel combustion and forest burning) (Text S1; Figs. S1 and S2) (Massling et al., 2015; Chen et al., 2016b).

2.5. Air mass origin, chlorophyll-*a* concentration, and meteorological parameters

Both 8-day and monthly mean Chl-*a* concentration data level-3 MODIS Aqua were downloaded from the NASA OCEAN Color website (http://oceancolor.gsfc.nasa.gov/) at a 4-km resolution. The three-dimensional 5-d (120 h) back trajectories were calculated using the Hybrid Single-Particle Lagrangian Integrated Trajectory model from the NOAA Air Resources Laboratory (Draxler and Hess, 1998). Meteorological parameters including solar radiation, relative humidity, and air temperature at each time point were also calculated along the air mass trajectories. The calculations were made based on meteorological data from Global Data Assimilation System (at 1° latitude × 1° longitude resolution) produced by the National Centers for Environmental Prediction. Air masses were modelled to arrive at an altitude of 50 m above sea level at the Gruvebadet station at each hour of the study period. To identify the major air mass pathways prior to reaching to the Gruvebadet station, the calculated air mass trajectories were grouped into several clusters using the k-means clustering algorithm. Monthly mean air temperature data at 900 hPa were obtained from European Centre for Medium-Range Weather Forecasts Reanalysis 5 at a 30-km resolution. Sea level pressure data were obtained from the National Oceanic and Atmospheric Administration Physical Sciences Laboratory (http://psl.noaa.gov/).

The retention time for air masses in each domain type (including the ocean, marginal ice zone, multi-year ice, and land) was calculated based on the sea ice index at 25-km resolution provided by the National Snow and Ice Data Center (Choi et al., 2019). Note that the marginal ice zone and multi-year ice represent the areas in which the sea ice cover is 15−80% and > 80%, respectively (Stroeve et al., 2016). The air mass exposure to chlorophyll (E_{Chl}) was calculated to estimate the biological exposure history of air masses arriving at the observation site (Arnold et al., 2010; Park et al., 2018), according to Equation 5:

$$E_{Chl} = \frac{\sum_{t=1}^{120} Chl}{n} \tag{5}$$

where Chl is the 8-day mean Chl-*a* concentration within a radius of 25 km at a given time point (t) along the 5-day air mass back trajectory, and n is the total number of time points for which valid Chl-*a* values were available.

3. Results

3.1. Atmospheric DMS mixing ratio

The mixing ratio of atmospheric DMS, the precursor of Bio-SO_4^{2-} and MSA, showed considerable (several orders of magnitude) variability at daily to weekly intervals during the bloom and post-bloom periods (Figs. 2a and 3b). As confirmed in other studies (e.g. Arnold et al., 2010; Park et al., 2013; Mungall et al., 2016), the atmospheric DMS mixing ratio generally corresponded to the phytoplankton biomass in the oceans surrounding Svalbard (Figs. 2a and S3). During the bloom period the maximum monthly mean mixing ratio of DMS occurred in May 2015 (68.4 $\pm$ 86.8 pptv); an increase in the DMS mixing ratio continued until August of that year, reflecting the persistent phytoplankton biomass producing DMS in the vicinity of Svalbard. Based on our atmospheric DMS concentration data, we conclude that DMS was ubiquitous in the Arctic atmosphere for the entire period of warming from the phytoplankton bloom to post-bloom periods (Park et al., 2013).

3.2. S isotopic composition (δ^{34}S) and sources of sulfate aerosols

The δ^{34}S values for sulfate aerosols ranged from 2.2 to 17.6 ‰ between March and August (Fig. 2b). In all years of measurement, the δ^{34}S values were low in April or earlier months, rapidly increased towards May to June, and remained high towards August (Fig. 3c). As warming progressed, the trend of increasing δ^{34}S in the sulfate aerosols was broadly consistent with the increasing mixing ratio of atmospheric DMS. The δ^{34}S values for the pre-bloom, bloom, and post-bloom periods averaged over five years were 7.5 $\pm$ 2.6 ‰, 9.5 $\pm$ 2.8 ‰, and 11.3 $\pm$ 2.8 ‰, respectively, reflecting an increasing enrichment in the heavier ^{34}S towards summer. The maximum monthly mean δ^{34}S (13.5 $\pm$ 2.6 ‰) occurred in July 2018, whereas the lowest mean (3.7 $\pm$ 1.8 ‰) occurred in April 2019. The mean pre-bloom δ^{34}S value in 2017 (9.2 $\pm$ 1.8 ‰) was higher than in 2018 (5.9 $\pm$ 1.2 ‰), whereas the mean bloom and post-bloom δ^{34}S values were marginally lower in 2017 (11.0 $\pm$ 2.0 ‰) than in 2018 (12.5 $\pm$ 2.8 ‰).

On monthly scales the greatest contribution of Bio-SO_4^{2-} occurred in August 2018 (59.4 $\pm$ 17.2 %) (Fig. S4). The proportion of Bio-SO_4^{2-} among all SO_4^{2-} particles was 18.1 $\pm$ 16.6 % during the pre-bloom period, and then sharply increased to 37.2 $\pm$ 21.0 % during the bloom and post-bloom periods, whereas the contribution of anthropogenic SO_2 was 79.2 $\pm$ 16.9 % during the pre-bloom period and 57.9 $\pm$ 21.4 % during the bloom and post-bloom periods. Anth-SO_4^{2-} was found to be the largest contributor to total SO_4^{2-} during all three periods (Fig. S4), which was consistent with the previous findings (Li and Barrie, 1993; Norman et al., 1999; Udisti et al., 2016).

3.3. NSS-SO_4^{2-}, Anth-SO_4^{2-}, and Biogenic sulfur aerosols

There were considerable seasonal and interannual variations in the concentrations of S aerosols including NSS-SO_4^{2-}, Anth-SO_4^{2-}, and Bio-S-aerosol (Figs. 3d–h, 4 and 5). In all years of the study the seasonal mean NSS-SO_4^{2-}

concentration reached a maximum during the pre-bloom period (857 ± 520 ng m^{-3}), decreased rapidly towards summer, and eventually dropped to a quarter of the maximum value during the post-bloom period (212 ± 120 ng m^{-3}). We also found that the NSS-SO$_4^{2-}$ concentration in the months prior to May varied by as much as a factor of three (1015 ± 586 in 2015 versus 291 ± 93 ng m^{-3} in 2019). The highest monthly mean NSS-SO$_4^{2-}$ concentration (1309 ± 131 ng m^{-3}) was recorded in March 2017, and the lowest was in July 2018 (165 ± 128 ng m^{-3}). The concentration of Anth-SO$_4^{2-}$ showed a temporal trend similar to that of NSS-SO$_4^{2-}$, with the highest monthly mean concentration (678 ± 450 ng m^{-3}) occurring during the pre-bloom period, followed by a trend of decrease for the bloom (369 ± 236 ng m^{-3}) and post-bloom (114 ± 78 ng m^{-3}) periods.

During the pre-bloom period, when the chlorophyll-*a* concentration remained lower than 0.5 mg m^{-3} in waters around Svalbard, the concentration of Bio-SO$_4^{2-}$ was unexpectedly high (180 ± 213 ng m^{-3}), reaching 743 ng m^{-3} in 2016 (Fig. 4c). During the phytoplankton bloom period, the seasonal mean concentration of Bio-SO$_4^{2-}$ was highest (184 ± 190 ng m^{-3}). As summer approached, the Bio-SO$_4^{2-}$ concentration decreased slightly during the post-bloom periods (98 ± 68 ng m^{-3}; Fig. 4c). In contrast to the trend for Bio-SO$_4^{2-}$, the MSA concentration remained low (< 30 ng m^{-3}) during the pre-bloom period, and rapidly increased during the transition from the pre-bloom to bloom periods (Figs. 3g and 5a). An elevated MSA concentration maintained during much of the bloom and post-bloom periods, and then it decreased slightly to near the detection limit by the end of August. The highest monthly mean MSA concentrations were found in May (81.4 ± 58.1 ng m^{-3}) and June (81.9 ± 56.5 ng m^{-3}), which broadly agree with previous MSA measurements at Svalbard (Becagli et al., 2019). The annual mean concentrations of MSA (March to August) varied slightly among years (46.2 ± 35.9 ng m^{-3} in 2017, 63.5 ± 52.9 ng m^{-3} in 2018, and 55.4 ± 45.5 ng m^{-3} in 2019). The Bio-S-aerosol concentration increased with the onset of the spring bloom, and stayed at moderate levels until June (Figs. 3h and 5b). The concentration of Bio-S-aerosol during the bloom period (252 ± 197 ng m^{-3}) was slightly higher than that during post-bloom period (149 ± 91 ng m^{-3}), and the highest monthly concentration of Bio-S-aerosol was found in April or May in all measurement years. The total concentrations of Bio-S-aerosol during the bloom and post-bloom periods were comparable in all three years (214 ± 124 ng m^{-3} in 2017, 204 ± 174 ng m^{-3} in 2018, and 160 ± 153 ng m^{-3} in 2019).

3.4. Ratio of MSA to Bio-S-aerosol (R_{Bio})

In all years of this study the R_{Bio} values derived from δ^{34}S data were lowest during the pre-bloom period and increased in the transition to the spring bloom, as biogenic DMS production peaked (Figs. 3i and 5c). The R_{Bio} value varied by a factor of three over seasons, showing maximum values during the bloom period (0.32 ± 0.17), and lowest values during the pre-bloom period (0.09 ± 0.07). The highest mean R_{Bio} (0.49 ± 0.05) was found in June 2018, whereas the lowest R_{Bio} (0.08 ± 0.01) was found in March 2017. There were large interannual variations in the seasonal mean R_{Bio} (0.24 ± 0.11 in 2017, 0.40 ± 0.14 in 2018, and 0.36 ± 0.14 in 2019) during the bloom and post-bloom periods.

Similar R_{Bio} values were also reported at Ny-Ålesund. For example, Udisti et al (2016) reported a MSA to Bio-SO$_4^{2-}$ ratio of 0.33 (R_{Bio} = 0.25) during the spring-summer period in 2014. This ratio was derived from a multi-seasonal asymptotic value in a plot between the MSA to NSS-SO$_4^{2-}$ ratio and the MSA concentration. Implicit in this calculation is the assumption that the fraction of Bio-SO$_4^{2-}$ in the total NSS-SO$_4^{2-}$ aerosols is overwhelming when the MSA to NSS-SO$_4^{2-}$ ratio approaches the asymptotic value (Udisti et al., 2016; Park et al., 2017). Other investigators also reported comparable R_{Bio} values in other Arctic environments: 0.18–0.20 at the central Arctic Ocean (Chang et al., 2011b; Leck and Persson 1996); 0.28 at the Eastern Antarctic Plateau (Udisti et al., 2012); and 0.28 at Alert (Norman et al., 1999). These R_{Bio} values were all derived from a multi-seasonal asymptotic value in a plot between the MSA to NSS-SO$_4^{2-}$ ratio and MSA concentration. The analytical accessibilities associated with measurements of MSA and NSS-SO$_4^{2-}$ concentration (i.e., less laborious and requires fewer aerosols than is needed for the technique measuring the S-isotope ratio) make data on the MSA to NSS-SO$_4^{2-}$ ratio more widely available.

4. Discussion

4.1. Factors affecting variations in the S aerosol concentration in the Arctic atmosphere

Seasonal variations in NSS-SO$_4^{2-}$ aerosols were strongly associated with variations in Anth-SO$_4^{2-}$. In particular, the tight association of these parameters indicates that Anth-SO$_4^{2-}$ aerosols were the largest contributor to NSS-SO$_4^{2-}$ during the pre-bloom period, when the intrusion of Arctic haze is considerable (Figs. S4 and S5). During the transition from the pre-bloom to bloom periods, the input of Anth-SO$_4^{2-}$ particles to our study area rapidly decreased because of weakening of the northward transport of air masses (containing Anth-SO$_4^{2-}$) from Europe and increasing removal of Anth-SO$_4^{2-}$ aerosols by increasing precipitation as the seasons progress (Li and Barrie, 1993) (Fig. 4b). The decreasing input of Anth-SO$_4^{2-}$ particles to the observation site during the bloom and post-bloom periods was also independently confirmed by the trend of decrease in the measured black carbon concentration at our observation site (Figs. 3a and S2).

The large interannual variability in NSS-SO$_4^{2-}$ from March to April was strongly associated with changes in the trajectory of the air masses reaching Svalbard, and the sea level pressure along those air mass trajectories (Fig. 6). More explicitly, the higher concentrations of NSS-SO$_4^{2-}$ particles in 2015 (1015 $\pm$ 586 ng m^{-3}) resulted from the greater input of pollutants (Anth-SO$_4^{2-}$) from northern Europe via the intensified south-westerly wind, whereas the opposite occurred in 2018 and 2019 (634 $\pm$ 266 for 2018 and 291 $\pm$ 93 ng m^{-3} for 2019).

Unusual elevation of the Bio-SO$_4^{2-}$ concentration was occasionally found in the oceans surrounding Svalbard during the pre-bloom period in 2016 and 2017, despite low biological activity (as indicated by DMS mixing ratios of < 10 pptv) (Figs. 4c and S6). The spikes in the Bio-SO$_4^{2-}$ concentration likely originate from Bio-SO$_4^{2-}$ aerosols that were produced in distant ocean regions (e.g., the North Atlantic Ocean, the Norwegian Sea, and further south of 50° N–70° N and

25° W–50° E), and then carried into the Arctic via a northward transport of air masses. Analysis of air mass back trajectory
275 data showed that the elevated values of Bio-SO_4^{2-} during the pre-bloom period in 2016 and 2017 resulted from air masses from lower latitude regions reaching Svalbard, rather than originating locally from the oceans around Svalbard, while the much lower Bio-SO_4^{2-} concentrations in 2018 probably resulted from an absence of air masses originating from distant DMS source regions during the pre-bloom period (Figs. 4c and S7).

The MSA concentration remained low during the pre-bloom period (i.e., no apparent high peaks), largely because
280 of the greater removal of MSA relative to Bio-SO_4^{2-} aerosols during long-range transport to Svalbard from the distant source regions to the south. For example, MSA tends to more easily condense onto existing particles (Hoppel, 1987; Pszenny et al., 1989) because of its higher vapor pressure, and is thus more rapidly removed from the atmosphere with larger particles through wet deposition; this results in greater loss of MSA relative to SO_4^{2-}. Greater enrichment of MSA occurs in super-micron sized particles than in submicron particles (Legrand and Pasteur, 1998). The higher ratios of MSA to NSS-SO_4^{2-} in
285 rainwater and fresh snow than in aerosol particles is also indicative of the greater removal of MSA (Berresheim et al., 1991; Jaffrezo et al., 1994). The production mechanism of MSA (via DMS oxidation by OH radicals) (Gondwe et al., 2004) could also lower the MSA concentration during the pre-bloom period, when the low levels of OH radicals (as a result of low light conditions) resulted in less MSA production. The elevations of MSA occurred in May or June, when the production of OH radicals was high and associated with increasing solar radiation and biological production (Fig. S8 and S9a).

290 The concentrations of Bio-S-aerosol during the bloom and post-bloom periods were comparable in all three years (214 $\pm$ 124 ng m^{-3} in 2017, 204 $\pm$ 174 ng m^{-3} in 2018, and 160 $\pm$ 153 ng m^{-3} in 2019), despite differing phytoplankton biomass (derived from Chl-a) among those years (Fig. S9b). This mismatch has been reported previously, and suggests that estimations of marine organic aerosols based on Chl-a data only are unreliable (Rinaldi et al., 2013). In particular, the summer DMS-driven aerosols produced from the Barents Sea were not proportional to the Chl-a concentrations (Becagli et
295 al., 2016). Different compositions of phytoplankton species in different ocean domains (Greenland Sea versus Barents Sea) could also result in changes in DMS production because phytoplankton have differing cellular levels of dimethylsulfoniopropinate (DMSP; a precursor of DMS) and the DMSP cleavage enzyme (enabling the transformation of DMSP to DMS) (Park et al., 2014b). The DMS production capacity in the Greenland Sea (where prymnesiophytes dominate) was found to be 3-fold higher than that in the Barents Sea (where diatoms dominate) (Park et al., 2018). Other studies have
300 also reported that the concentrations of MSA or Bio-SO_4^{2-} do not always follow the atmospheric DMS mixing ratio, highlighting the involvement of other factors in the oxidation of DMS to MSA or Bio-SO_4^{2-} (Read et al., 2008; Yan et al., 2020a). Therefore, the amounts of DMS produced and its oxidation products may not be solely explained by variations in the ocean biomass.

In the Arctic summer atmosphere the low abundance of large particles (i.e., Aitken and accumulation mode) could
305 probably enhance the formation of new particles via the gas-to-particle conversion process and the ultimate initiation of CCN formation (Boy et al., 2005; Dall'Osto et al., 2018). The concurrent increase in biogenic sulfate aerosols and small

sized particles (3–10 nm and 10–100 nm, respectively) reported for the Arctic atmosphere in May (Park et al., 2017) is a prime example that biogenic DMS is a major contributor to NPF. A model study reported that DMS enhanced the mass of sulfate particles in the size range 50–100 nm in regions north of 70° N (Ghahremaninezhad et al., 2019). During the bloom and post-bloom periods a decline in anthropogenic sources and an increase in oceanic DMS source strength resulted in the transition of major sulfate sources from Anth-SO_4^{2-} to Bio-SO_4^{2-}, which highlights the increasing importance of biogenic sulfur aerosols in the summer Arctic atmosphere. Biogenic organic aerosols in the high Arctic were reported to contribute considerably to the concentrations of ultrafine and CCN particles from summer to early autumn when anthropogenic source is lowest (Dall'Osto et al., 2017; Lange et al., 2019). Nonetheless, Anth-SO_4^{2-} contributed considerably to the total SO_4^{2-} budget during the post-bloom period, indicating that even in summer the Anth-SO_4^{2-} transported from Europe or local emissions can exert a significant influence on the sulfate budget in the Arctic atmosphere (Fig. S4) (Chen et al., 2016b; Gogoi et al., 2016; Dekhtyareva et al., 2018).

4.2. Factors influencing the DMS oxidation pathways to either MSA or Bio-SO_4^{2-} (R_{Bio})

4.2.1. Seasonal variations in R_{Bio}

Our data spanning five years show two distinctive trends in R_{Bio} among seasons or years. The first is that the values of R_{Bio} during the bloom and post-bloom periods (0.32 ± 0.15) were a factor of three higher than the pre-bloom values (0.09 ± 0.07) (Fig. 5c). The large seasonal difference in R_{Bio} could be explained by known factors including the concentration of OH radicals (directly influenced by light intensity), air temperature (determining the oxidation pathway of DMS to either MSA or Bio-SO_4^{2-}), the chemical properties of existing particles (e.g., the black carbon concentration) (e.g., Saltzman et al., 1986; Gondwe et al., 2004; Yan et al., 2020b), and biological activities near observation site. Among those, a major factor is the concentration of OH radicals. BrO radicals also help facilitate the addition pathway in the oxidation of DMS, even at concentrations > 1 pptv level (von Glasow and Crutzen, 2004). It has been hypothesized that the reactive bromines produced photochemically and heterogeneously at sea ice and snowpack surfaces lead to the BrO enrichment over ice-covered regions (Abbatt et al., 2012; Fernandez et al., 2019). Therefore, a high light intensity would favor the oxidation pathway of DMS to MSA, because this pathway is effectively mediated by photochemically activated species including OH and BrO. The solar radiation (51.3 ± 36.1 W m^{-2}) over the distant DMS source regions during the pre-bloom period was much lower than over the Greenland Sea and the Barents Sea during the bloom (243.0 ± 63.4 W m^{-2}) and post-bloom (222.5 ± 70.5 W m^{-2}) periods (Fig. 7). The low OH radical and reactive bromine concentrations during the pre-bloom period probably lowered the production of MSA from DMS oxidation (i.e., weakening the addition pathway), and thereby resulted in the lower R_{Bio} value (0.09 ± 0.07) than was found during the bloom (0.32 ± 0.17) and post-bloom (0.32 ± 0.13) periods (Table S2). Consequently, solar radiation was likely to be a major driver of the seasonal R_{Bio} change in the Arctic atmosphere.

The chemical properties of existing particles could influence the seasonal variations in R_{Bio}. Explicitly, the uptake of gaseous MSA onto particles was found to be sensitive to the chemical properties of those particles (Yan et al., 2020b). In particular, hydrophobic and acidic particles in the atmosphere tended to hinder the adhesion of gaseous MSA to particles,

340 while alkaline sea-salt particles tended to accelerate the adhesion process (Pszenny, 1992; Jefferson et al., 1998; Yan et al., 2020b). Elemental carbon particles emitted from fossil fuel combustion are highly hydrophobic, and sulfates in the aerosol particles are acidic. However, only a small proportion of the anthropogenic particles formed in the polluted coastal and urban sites was found to be associated with MSA (Gaston et al., 2010; Yan et al., 2020) formed from the oxidation of aqueous DMS catalyzed by iron and vanadium (Gaston et al., 2010; Moffett et al., 2020). Therefore, the air masses (rich in black

345 carbon and sulfate) that originate from northern Europe probably have PM 2.5 particles containing low MSA concentrations, despite the fact that those air masses swept through productive ocean areas during the pre-bloom period (Fig. 5a). In contrast, during the bloom period we found an elevation of the MSA concentration, primarily as a result of two reinforcing processes: the greater DMS oxidation to MSA, and the enhanced condensation of gaseous MSA to the existing particles under less hydrophobic and acidic conditions. For each group of R_{Bio} values, the lower concentrations of black carbon and sulfate

350 resulted in the greater uptake of gaseous MSA, and thereby resulted in higher R_{Bio} values (Fig. 8). We also found significant inverse correlations between black carbon and R_{Bio} ($r = -0.79$; Fig. 9a) and between total SO_4^{2-} and R_{Bio} ($r = -0.73$; Fig. 9b); these tight correlations substantiate the importance of the chemical properties of atmospheric particles in determining the rate of uptake of gaseous MSA by the particles present in air. The number of samples measured during the bloom and post-bloom periods was higher in the groups having large R_{Bio} values (Fig. 8c).

355 A strong positive correlation between monthly mean R_{Bio} and the air mass exposure to chlorophyll (E_{Chl}) was observed during the study period ($r = 0.82$). The retention time of air masses over the ocean and marginal ice zone (i.e., DMS source regions) was also positively correlated with R_{Bio} values ($r = 0.54$). The R_{Bio} values decreased with decreasing air mass retention time over the land and multi-year ice regions (i.e., the non-DMS-source regions). The concentration of MSA was positively correlated with the mean Chl-a concentration in areas surrounding the observation site, but no similar

360 clear correlation was found between Bio-SO_4^{2-} and Chl-a (Fig. S9). The absence of a correlation between Bio-SO_4^{2-} and Chl-a indicates that the concentration of Bio-SO_4^{2-} measured at the observation site included sulfur compounds produced locally and in distant regions, because the greater atmospheric residence time of Bio-SO_4^{2-} (relative to MSA) indicates greater intrusion of Bio-SO_4^{2-} into the observation site. Hence, air masses that have been extensively exposed to local biological activities are likely to have higher R_{Bio} values. Therefore, the seasonal variations in R_{Bio} measured at Ny-Ålesund

365 were probably controlled by the concentration of OH radicals (largely determined by light intensity), the chemical properties of the particles containing black carbon and sulfates, and biological activities surrounding the observation site. Another established factor that could affect the seasonal variations in R_{Bio} is air temperature. However, we found no association between R_{Bio} and air temperature (see Text S2).

The R_{Bio} values in the present study, and those determined in other high latitude regions including Barrow in Alaska
370   (USA) and Neumayer station in the Antarctic coastal region, consistently pointed to the highest R_{Bio} values occurring in
summer (Li et al., 1993; Legrand and Pasteur, 1998; Norman et al., 1999). We found that seasonal variability in R_{Bio}
measured in the Arctic region can be better explained by light conditions, the chemical properties of particles, and biological
activities near the observation site than by air temperature. Specifically, the R_{Bio} values measured during the pre-bloom
period poorly represent the oxidative conditions of DMS in the Arctic atmosphere, because of the considerable intrusion of
375   anthropogenic pollutants from the distant northern Europe. Thus, the R_{Bio} values measured during the bloom and post-bloom
periods probably more accurately represent the ratio of the oxidation products of DMS produced in the ocean regions
surrounding Svalbard under the less polluted conditions of the Arctic atmosphere.

4.2.2 Interannual variations in R_{Bio}

The second distinctive trend is the interannual difference in R_{Bio}. The R_{Bio} values measured in 2017 were much
380   lower than the values in other years (2015, 2016, 2018, and 2019; Fig. 10). One explanation for large interannual variations
in R_{Bio} is the difference in the condensation of gaseous MSA onto particles in the Arctic atmosphere. As noted above, the
chemical properties of particles largely determines the rate of MSA condensation onto them (Jefferson et al., 1998; Yan et
al., 2020b). During the pre-bloom and bloom periods in 2017, higher concentrations of black carbon and sulfate were found
relative to other years, and consequently, lower R_{Bio} values found in 2017 (Fig. 10). However, we found no discernible
385   interannual difference in the concentrations of black carbon (8.3 ± 4.9 ng m^{-3} in 2017, and 9.5 ± 6.1 ng m^{-3} in other years)
and total SO_4^{2-} (235 ± 101 ng m^{-3} in 2017, and 232 ± 134 ng m^{-3} in the other years) during the post-bloom period (Fig.
10f). To our surprise, during the post-bloom period the R_{Bio} value (0.22 ± 0.07) in 2017 was only half the rate measured in
the other years (0.39 ± 0.11). The lack of an association of black carbon and sulfate concentrations with R_{Bio} values indicates
that factors other than chemical properties of existing particles affected the interannual variation in R_{Bio} values measured
390   during the post-bloom period.

Air temperature difference may explain the interannual variations in R_{Bio} during the post-bloom period (Fig. S11).
However, the lack of correlation (e.g. Bates et al., 1992b) we found between R_{Bio} values and the mean temperatures of air
masses along the entire pathway to Svalbard (Fig. S11b) is consistent with the results of other studies (Savoie et al., 1992;
Legrand and Pasteur, 1998; Zhan et al., 2017; Moffett et al., 2020), implying that variations in air temperature were not a
395   driver of determining the DMS branching ratio. We also found no discernible differences in solar radiation and relative
humidity between year of 2017 and other years, thus neither solar radiation nor relative humidity showed any association
with R_{Bio} (Fig. S11c–d). Thus, no meteorological factors adequately explain the interannual variations in R_{Bio} during the post-
bloom period. The concurrent measurements of DMS and MSA during summer in the Southern Ocean reinforce our finding
that temperature and relative humidity have negligible effects on the conversion of DMS to MSA (Yan et al., 2020a).

400   Analysis of air mass back-trajectory data indicated that the air mass exposure to chlorophyll (E_{Chl}) in 2017 (0.44 ± 0.21) was 30% lower than in other years (0.63 ± 0.35). The mean retention time of air masses over the sea ice and land areas (i.e., non-DMS source regions) in 2017 (40.9 ± 27.9 h) was 25% longer than that estimated for other years (32.3 ± 19.2 h), whereas the mean retention time of air masses over the ocean and marginal ice regions (i.e., the DMS source regions) was lower in 2017 (79.1 ± 27.9 h) than in other years (87.7 ± 19.2 hours) (Fig. 11). Hence, the 2017 R_{Bio} values were 40% lower

405   than those in 2018 and 2019, probably because more air masses swept over non-DMS source regions.

As sulfate and MSA particles have different roles in terms of particle formation and growth, the importance of R_{Bio} is worth highlighting. Sulfate particles (including sulfuric acids) are known to produce 4–6 times more submicron sized particles than MSA, leading to a 10-fold stronger cooling effect via scattering of solar radiation (i.e., a direct effect), whereas the impacts of sulfate and MSA particles on cloud microphysics (i.e., an indirect effect) are comparable (Hodshire et al.,

410   2019). Our findings of considerable seasonal or interannual variations in R_{Bio} indicate that the conventional approach of using asymptotic values to determine the oxidation products of DMS and to evaluate the contribution of biogenic sources to the total sulfur budget at particular locations (e.g., Norman et al., 1999; Udisti et al., 2012 and 2016) is problematic.

5. Conclusion and Implication

This study shows that in the Arctic atmosphere extensive production of the oxidation products of DMS (i.e., Bio-

415   SO_4^{2-} and MSA) occurred from the onset to the termination of phytoplankton blooms between 2015 and 2019. Anth-SO_4^{2-} was found to be the largest contributor to total sulfate aerosols during the pre-bloom periods, as a result of the influence of Arctic haze. Its contribution was comparable to that of Bio-SO_4^{2-} during the bloom and post-bloom periods. We also found large interannual variations in anthropogenic and biogenic sulfur aerosols. Moreover, the ratio of MSA to Bio-SO_4^{2-} (R_{Bio}) tended to be higher (0.32 ± 0.15) in summer than in early spring (0.09 ± 0.07), Our results imply that NPF, and subsequent

420   growth of those particles to form CCN, are governed by both Bio-SO_4^{2-} and MSA when R_{Bio} is high (bloom and post-bloom periods), but that when R_{Bio} is low (pre-bloom period) MSA makes only a small contribution to particle growth and other molecules with low-volatility vapors (e.g., highly oxygenated organic molecules) are more involved in particle growth near Svalbard. The large interannual variability of R_{Bio} further indicates that condensational growth following NPF can be affected by MSA or other molecules with low-volatility vapors, depending on the branching ratio of DMS oxidation.

425   In modelling studies (Vallina et al., 2006, 2007) the annual contribution of biogenically induced CCN to total global CCN has been estimated to be greater than 30 %, and up to 80 % in the austral summer in the Southern Ocean. This is similar to findings for the Northern hemisphere, where Bio-SO_4^{2-} particles accounted for greater than 60 % of CCN in late spring (May and June) in the North Atlantic (Sanchez et al., 2018). An acceleration of sea ice retreat and an increase in melt ponds in the Arctic Ocean will increase biogenic DMS production, resulting in a greater contribution of biogenic S aerosols

430   to atmospheric aerosol formation and climate regulation (Arrigo et al., 2008; Gourdal et al., 2018; Park et al., 2019; Galí et al., 2019). Another important factor that may be involved in the formation of biogenic CCN is changes in the atmospheric

concentrations of OH, NO_x and BrO; these are likely to be affected by future climate change and increasing anthropogenic perturbations (e.g., sea ice decline, increasing reduced carbon emissions) (Alexander and Mickley, 2015). Our measurements primarily focused on the particle phase of sulfur species (particles < 2.5 μm), but did not cover the initial phase of DMS

435 oxidation and particle growth (i.e. nano size scales), including the concentration of the oxidants and gas-phase composition of sulfur species. Therefore, the integrated study of both the gas and particle phases of sulfur compounds (including gaseous MSA, SO_4^{2-}, and hydroperoxymethyl thioformate), ocean colors, and sea ice properties will help define the climate-relevant impacts of oxidation products of biogenic DMS in the Arctic environment.

Data availability

440   All data needed to draw the conclusions in the present study are presented in this report and/or the Supplementary Materials. For additional data related to this study, please contact the corresponding author (Kitack Lee; ktl@postech.ac.kr).

Supplement

The supplement related to this article is available on line at https://

Author contributions

445   S.J., K.P., Y.Y., and K.L. designed the data analysis and wrote the manuscript. S.J., K.P. and E.J. performed the data evaluation and analyses. K.K. and H.C. performed the ion chromatograph measurements. K.E. provided the black carbon data. R.T. and S.B. were involved in aerosol sample collection. B.L., R.K., and O.H. contributed to the interpretation of the results.

Competing interests

450   The authors declare that they have no conflict of interest.

Acknowledgements

This research was supported by National Research Foundation of Korea funded by the Ministry of Science and ICT (Basic Research Program; NRF-2020R1A4A1018818) and KOPRI-PN21011 (NRF-2021M1A5A1065425).

References

455   Abbatt, J. P. D., Thomas, J. L., Abrahamsson, K., Boxe, C., Granfors, A., Jones, A. E., King, M. D., Saiz-Lopez, A., Shepson, P. B., Sodeau, J., Toohey, D. W., Toubin, C., von Glasow, R., Wren, S. N., and Yang, X.: Halogen activation via interactions with environmental ice and snow in the polar lower troposphere and other regions, Atmos. Chem. Phys., 12, 6237–6271, https://doi.org/10.5194/acp-12-6237-2012, 2012.

Albrecht, B. A.: Aerosols, cloud microphysics, and fractional cloudiness, Science, 245(4923), 1227–1230,

460   https://doi.org/10.1126/science.245.4923.1227, 1989.

Alexander, B., and Mickley, L. J.: Paleo-perspectives on potential future changes in the oxidative capacity of the atmosphere due to climate change and anthropogenic emissions, Current Pollution Reports, 1(2), 57–69, https://doi.org/10.1007/s40726-015-0006-0, 2015.

Arnold, S. R., Spracklen, D. V., Gebhardt, S., Custer, T., Williams, J., Peeken, I., and Alvain, S.: Relationships between

465   atmospheric organic compounds and air-mass exposure to marine biology, Environ. Chem., 7(3), 232–241, https://doi.org/10.1071/EN09144, 2010.

Arrigo, K. R., van Dijken, G., and Pabi, S.: Impact of a shrinking Arctic ice cover on marine primary production, Geophys. Res. Lett., 35(19), L19603, https://doi.org/10.1029/2008GL035028, 2008.

Ayers, G. P., Ivey, J. P., and Gillett, R. W.: Coherence between seasonal cycles of dimethyl sulphide, methanesulphonate

470   and sulphate in marine air, Nature, 349(6308), 404–406, https://doi.org/10.1038/349404a0, 1991.

Bates, T. S., Lamb, B. K., Guenther, A., Dignon, J., and Stoiber, R. E.: Sulfur emissions to the atmosphere from natural sources, J. Atmos. Chem., 14(1-4), 315–337, https://doi.org/10.1007/BF00115242, 1992a.

Bates, T. S., Calhoun, J. A., and Quinn, P. K.: Variations in the methanesulfonate to sulfate molar ratio in submicrometer marine aerosol particles over the South Pacific Ocean, J. Geophys. Res.-Atmos., 97(D9), 9859–9865,

475   https://doi.org/10.1029/92JD00411, 1992b.

Barnes, I., Hjorth, J., and Mihalopoulos, N.: Dimethyl sulfide and dimethyl sulfoxide and their oxidation in the atmosphere, Chem. Rev., 106, 940–975, https://doi.org/10.1021/cr020529, 2006.

Becagli, S., Lazzara, L., Marchese, C., Dayan, U., Ascanius, S. E., Cacciani, M., Caiazzo, L., Di Biagio, C., Di Iorio, T., di Sarra, A., Eriksen, P., Fani, F., Giardi, F., Meloni, D., Muscari, G., Pace, G., Severi, M., Traversi, R., and Udisti, R.:

480   Relationships linking primary production, sea ice melting, and biogenic aerosol in the Arctic, Atmos. Environ., 136, 1–15, https://doi.org/10.1016/j.atmosenv.2016.04.002, 2016.

Becagli, S., Amore, A., Caiazzo, L., Iorio, T. D., Sarra, A. D., Lazzara, L., Marchese, C., Meloni, D., Mori, G., Muscari, G., Nuccio, C., Pace, G., Severi, M., and Traversi, R.: Biogenic Aerosol in the Arctic from Eight Years of MSA Data from Ny Ålesund (Svalbard Islands) and Thule (Greenland), Atmosphere, 10(7), 349,

485   https://doi.org/10.3390/atmos10070349, 2019.

Berresheim, H., Andreae, M. O., Ayers, G. P., Gillett, R. W., Merrill, J. T., Davis, V. J., and Chameides, W. L.: Airborne measurements of dimethylsulfide, sulfur dioxide, and aerosol ions over the Southern Ocean south of Australia, J. Atmos. Chem., 10(3), 341–370, https://doi.org/10.1007/BF00053868, 1990.

Berresheim, H., Andreae, M. O., Iverson, R. L., and Li, S. M.: Seasonal variations of dimethylsulfide emissions and atmospheric sulfur and nitrogen species over the western north Atlantic Ocean, Tellus B, 43(5), 353–372, https://doi.org/10.1034/j.1600-0889.1991.t01-1-00001.x-i1, 1991.

Bork, N., Elm, J., Olenius, T., and Vehkamäki, H.: Methane sulfonic acid-enhanced formation of molecular clusters of sulfuric acid and dimethyl amine, Atmos. Chem. Phys., 14(22), 12023–12030, https://doi.org/10.5194/acp-14-12023-2014, 2014.

Boy, M., Kulmala, M., Ruuskanen, T. M., Pihlatie, M., Reissell, A., Aalto, P. P., Keronen, P., Dal Maso, M., Hellen, H., Hakola, H., Jansson, R., Hanke, M., and Arnold, F.: Sulphuric acid closure and contribution to nucleation mode particle growth, Atmos. Chem. Phys., 5, 863–878, https://doi.org/10.5194/acp-5-863-2005, 2005.

Böttcher, M. E., Brumsack, H.-J., and Dürselen, C.-D.: The isotopic composition of modern seawater sulfate: I. Coastal waters with special regard to the North Sea, J. Marine Syst., 67, 73–82, https://doi.org/10.1016/j.jmarsys.2006.09.006, 2007.

Burkart, J., Willis, M. D., Bozem, H., Thomas, J. L., Law, K., Hoor, P., Aliabadi, A. A., Köllner, F., Schneider, J., Herber, A., Abbatt, J. P. D., and Leaitch, W. R.: Summertime observations of elevated levels of ultrafine particles in the high Arctic marine boundary layer, Atmos. Chem. Phys., 17, 5515–5535, https://doi.org/10.5194/acp-17-5515-2017, 2017.

Chang, R. Y.-W., Sjostedt, S. J., Pierce, J. R., Papakyriakou, T. N., Scarratt, M. G., Michaud, S., Levasseur, M., Leaitch, W. R., and Abbatt, J. P. D.: Relating atmospheric and oceanic DMS levels to particle nucleation events in the Canadian Arctic, J. Geophys. Res.-Atmos., 116, D00S03, https://doi.org/10.1029/2011JD015926, 2011a.

Chang, R. W., Leck, C., Graus, M., Müller, M., Paatero, J., Burkhart, J. F., ... & Hansel, A.: Aerosol composition and sources in the central Arctic Ocean during ASCOS, Atmos. Chem. Phys., 11, 10619–10636, https://doi.org/10.5194/acp-11-10619-2011, 2011b.

Chen, L., Wang, J., Gao, Y., Xu, G., Yang, X., Lin, Q., and Zhang, Y.: Latitudinal distributions of atmospheric MSA and MSA/nss-SO_4^{2-} ratios in summer over the high latitude regions of the Southern and Northern Hemispheres, J. Geophys. Res., 117, D10306, https://doi.org/10.1029/2011JD016559, 2012.

Chen, H., Ezell, M. J., Arquero, K. D., Varner, M. E., Dawson, M. L., Gerber, R. B., and Finlayson-Pitts, B. J.: New particle formation and growth from methanesulfonic acid, trimethylamine and water, Phys. Chem. Chem. Phys., 17(20), 13699–13709, https://doi.org/10.1039/C5CP00838G, 2015.

Chen, H., Varner, M. E., Gerber, R. B., and Finlayson-Pitts, B. J.: Reactions of methanesulfonic acid with amines and ammonia as a source of new particles in air, J. Phys. Chem. B, 120(8), 1526–1536, https://doi.org/10.1021/acs.jpcb.5b07433, 2016a.

Chen, L., Li, W., Zhan, J., Wang, J., Zhang, Y., and Yang, X.: Increase in Aerosol Black Carbon in the 2000s over Ny-
520   Ålesund in the Summer, J. Atmos. Sci., 73(1), 251–262, https://doi.org/10.1175/JAS-D-15-0009.1, 2016b.

Choi, J. H., Jang, E., Yoon, Y. J., Park, J. Y., Kim, T. W., Becagli, S., Caiazzo, L., Cappelletti, D., Krejci, R., Eleftheriadis,
         K., Park, K.-T., and Jang, K. S.: Influence of biogenic organics on the chemical composition of Arctic aerosols,
         Global. Biogeochem. Cy., 33(10), 1238–1250, https://doi.org/10.1029/2019GB006226, 2019.

Coplen, T. B., and Krouse, H. R.: Sulphur isotope data consistency improved, Nature, 392(6671), 32–32,
525   https://doi.org/10.1038/32080, 1998.

Dall'Osto, M., Beddows, D. C. S., Tunved, P., Krejci, R., Ström, J., Hansson, H.-C., Yoon, Y. J., Park, K.-T., Becagli, S.,
         Udisti, R., Onasch, T., O'Dowd, C. D., Simó, R., and Harrison, R. M.: Arctic sea ice melt leads to atmospheric new
         particle formation, Sci. Rep., 7, 3318, https://doi.org/10.1038/s41598-017-03328-1, 2017.

Dall'Osto, M., Geels, C., Beddows, D. C. S., Boertmann, D., Lange, R., Nøjgaard, J. K., Harrison, R. M., Simo, R., Skov,
530   H., and Massling, A.: Regions of open water and melting sea ice drive new particle formation in North East
         Greenland, Sci. Rep., 8(1), 1–10, https://doi.org/10.1038/s41598-018-24426-8, 2018.

Dawson, M. L., Varner, M. E., Perraud, V., Ezell, M. J., Gerber, R. B., and Finlayson-Pitts, B. J.: Simplified mechanism for
         new particle formation from methanesulfonic acid, amines, and water via experiments and ab initio calculations, P.
         Natl. Acad. Sci., 109(46), 18719–18724, https://doi.org/10.1073/pnas.1211878109, 2012.

535 Dekhtyareva, A., Holmén, K., Maturilli, M., Hermansen, O., and Graversen, R.: Effect of seasonal mesoscale and microscale
         meteorological conditions in Ny-Ålesund on results of monitoring of long-range transported pollution, Polar Res.,
         37(1), 1508196, https://doi.org/10.1080/17518369.2018.1508196, 2018.

Draxler, R. R., and Hess, G. D.: An overview of the HYSPLIT_4 modelling system for trajectories, Aust. Meteorol. Mag.,
         47(4), 295–308, 1998.

540 Eleftheriadis, K., Vratolis, S., and Nyeki, S.: Aerosol black carbon in the European Arctic: measurements at Zeppelin station,
         Ny-Ålesund, Svalbard from 1998–2007, Geophys. Res. Lett., 36(2), https://doi:10.1029/2008GL035741, 2009.

Fernandez, R. P., Carmona-Balea, A., Cuevas, C. A., Barrera, J. A., Kinnison, D. E., Lamarque, J.-F., Blaszczak-Boxe, C.,
         Kim, K. T., Choi, W. Y., Hay, T., Blechschmidt, A.-M., Schönhardt, A., Burrows, J. P., and Saiz-Lopez, A.:
         Modeling the sources and chemistry of polar tropospheric halogens (Cl, Br, and I) using the CAM-Chem Global
545   Chemistry-Climate Model, J. Adv. Model. Earth. Sy., 11, 2259–2289, https://doi.org/10.1029/ 2019MS001655, 2019.

Galí, M., Devred, E., Babin, M., and Levasseur, M.: Decadal increase in Arctic dimethylsulfide emission, P. Natl. Acad.
         Sci., 116(39), 19311–19317, https://doi.org/10.1073/pnas.1904378116, 2019.

Gaston, C. J., Pratt, K. A., Qin, X., and Prather, K. A.: Real-time detection and mixing state of methanesulfonate in single
         particles at an inland urban location during a phytoplankton bloom, Environ. Sci. Technol., 44(5), 1566–1572,
550   https://doi.org/10.1021/es902069d, 2010.

Ghahremaninezhad, R., Gong, W., Galí, M., Norman, A. L., Beagley, S. R., Akingunola, A., Zheng, Q., Lupu, A., Lizotte, M., Levasseur, M., and Leaitch, W. R.: Dimethyl sulfide and its role in aerosol formation and growth in the Arctic summer–a modelling study, Atmos. Chem. Phys., 19(23), https://doi.org/10.5194/acp-19-14455-2019, 2019.

Gogoi, M. M., Babu, S. S., Moorthy, K. K., Thakur, R. C., Chaubey, J. P., and Nair, V. S: Aerosol black carbon over
555   Svalbard regions of Arctic, Polar Sci., 10(1), 60–70, https://doi.org/10.1016/j.polar.2015.11.001, 2016.

Gourdal, M., Lizotte, M., Massé, G., Gosselin, M., Poulin, M., Scarratt, M., Charette, J., and Levasseur, M.: Dimethyl sulfide dynamics in first-year sea ice melt ponds in the Canadian Arctic Archipelago, Biogeosciences, 15, 3169–3188, https://doi.org/10.5194/bg-15-3169-2018, 2018.

Gondwe, M., Krol, M., Klaassen, W., Gieskes, W., and de Baar, H.: Comparison of modeled versus measured MSA:nss
560        $SO_4^=$ ratios: A global analysis, Global. Biogeochem. Cy., 18(2), GB2006, https://doi.org/10.1029/2003GB002144, 2004.

Halas, S., and Szaran, J.: Improved thermal decomposition of sulfates to SO_2 and mass spectrometric determination of $\delta^{34}S$ of IAEA SO-5, IAEA SO-6 and NBS-127 sulfate standards, Rapid. Commun. Mass Sp., 15(17), 1618–1620, https://doi.org/10.1002/rcm.416, 2001.

565 Hayashida, H., Steiner, N., Monahan, A., Galindo, V., Lizotte, M., and Levasseur, M: Implications of sea-ice biogeochemistry for oceanic production and emissions of dimethyl sulfide in the Arctic, Biogeosciences, 14(12), https://doi.org/10.5194/bg-14-3129-2017, 2017.

Haywood, J., and Boucher, O.: Estimates of the direct and indirect radiative forcing due to tropospheric aerosols: A review, Rev. Geophys., 38(4), 513–543, https://doi.org/10.1029/1999RG000078, 2000.

570 Hodshire, A. L., Campuzano-Jost, P., Kodros, J. K., Croft, B., Nault, B. A., Schroder, J. C., Jimenez, J. L., and Pierce, J. R.: The potential role of methanesulfonic acid (MSA) in aerosol formation and growth and the associated radiative forcings, Atmos. Chem. Phys., 19(5), 3137–3160, https://doi.org/10.5194/acp-19-3137-2019, 2019.

Hoffmann, E. H., Tilgner, A., Schroedner, R., Bräuer, P., Wolke, R., and Herrmann, H.: An advanced modeling study on the impacts and atmospheric implications of multiphase dimethyl sulfide chemistry, P. Natl. Acad. Sci., 113(42), 11776–
575   11781, https://doi.org/10.1073/pnas.1606320113, 2016.

Hopkins, F. E., Suntharalingam, P., Gehlen, M., Andrews, O., Archer, S. D., Bopp, L., Bultenhuis, E., Dadou, I., Duce, R., Goris, N., Jickells, T., Johnson, M., Keng, F., Law, C. S., Lee, K., Liss, P. S., Lizotte, M., Malin, G., Murrell, J. C., Naik, H., Rees, A. P., Schwinger, J., and Williamson, P.: The impacts of ocean acidification on marine trace gases and the implications for atmospheric chemistry and climate, P. R. Soc. A., 476(2237), 20190769,
580   https://doi.org/10.1098/rspa.2019.0769, 2020.

Hoppel, W. A.: Nucleation in the MSA-water vapor system, Atmos. Environ., 21, 2703−2709, https://doi.org/10.1016/0004-6981(87)90202-2, 1987.

Hynes, A. J., Wine, P. H., and Semmes, D. H.: Kinetics and mechanism of hydroxyl reactions with organic sulfides, J. Phys. Chem., 90(17), 4148−4156, https://doi.org/10.1021/j100408a062, 1986.

585   IPCC: Climate Change 2013: The Physical Science Basis. Contribution of Working Group I to the Fifth Assessment Report of the Intergovernmental Panel on Climate Change, edited by: Stocker, T. F., Qin, D., Plattner, G.-K., Tignor, M., Allen, S. K., Boschung, J., Nauels, A., Xia, Y., Bex, V., and Midgley, P. M., Cambridge University Press, Cambridge, United Kingdom and New York, NY, USA, 1217–1308, 2013.

Jaffrezo, J. L., Davidson, C. I., Legrand, M., and Dibb, J. E.: Sulfate and MSA in the air and snow on the Greenland ice
590   sheet, J. Geophys. Res.-Atmos., 99(D1), 1241−1253, https://doi.org/10.1029/93JD02913, 1994.

Jang, S., Park, K.-T., Lee, K., and Suh, Y.-S.: An analytical system enabling consistent and long-term measurement of atmospheric dimethyl sulphide, Atmos. Environ., 134, 217–223, https://doi.org/10.1016/j.atmosenv.2016.03.041, 2016.

Jefferson, A., Tanner, D. J., Eisele, F. L., Davis, D. D., Chen, G., Crawford, J., Huey, J. W., Torres, A. L., and Berresheim,
595   H.: OH photochemistry and methane sulfonic acid formation in the coastal Antarctic boundary layer, J. Geophys. Res.-Atmos., 103(D1), 1647−1656, https://doi.org/10.1029/97JD02376, 1998.

Keene, W. C., Pszenny, A. P., Galloway, J. N., and Hawley, M. E.: Sea Salt Corrections and Interpretations of Constituent Ratios in Marine Precipitation, J. Geophys. Res., 91, 6647–6658, https://doi.org/10.1029/JD091iD06p06647, 1986.

Kettle, A. J. and Andreae, M. O.: Flux of dimethylsulfide from the oceans: A comparison of updated data sets and flux
600   models, J. Geophys. Res., 105, 26793–26808, https://doi.org/10.1029/2000JD900252, 2000.

Kim, J.-M., Lee, K., Yang, E. J., Shin, K., Noh, J. H., Park, K., Hyun B., Jeong, H.-J., Kim, J.-H., Kim, K. Y., Kim, M., Kim, H.C., Jang, P.-G., and Jang, M.C.: Enhanced production of oceanic dimethylsulfide resulting from CO_2-induced grazing activity in a high CO_2 world, Environ. Sci. Technol., 44, 8140–8143, https://doi.org/10.1021/es102028k, 2010.

605   Kulmala, M.: How Particles Nucleate and Grow, Science, 302, 1000–1001, https://doi.org/10.1126/science.1090848, 2003.

Kulmala, M., Vehkamäki, H., Petäjä, T., Dal Maso, M., Lauri, A., Kerminen, V.-M., Birmili, W., and McMurry, P.: Formation and growth rates of ultrafine atmospheric particles: a review of observations, J. Aerosol Sci., 35, 143–176, https://doi.org/10.1016/j.jaerosci.2003.10.003, 2004.

Krouse, H. R. and Grinenko, V. A.: Stable isotopes: natural and anthropogenic sulphur in the environment, 43, Wiley,
610   Chichester, UK, 1991.

Lange, R., Dall'Osto, M., Wex, H., Skov, H., and Massling, A.: Large summer contribution of organic biogenic aerosols to Arctic cloud condensation nuclei, Geophys. Res. Lett., 46(20), 11500–11509, https://doi.org/10.1029/2019GL084142, 2019.

Leaitch, W. R., Sharma, S., Huang L., Toom-Sauntry, D., Chivulescu, A., Macdonald, A. M., von Salzen, K., Pierce J. R.,
615   Bertram, A. K., Schroder, J. C., Shantz, N. C., Chang, R. Y.-W., and Norman A.-L.: Dimethyl sulfide control of the clean summertime Arctic aerosol and cloud, Elementa, 1, 00017, https://doi.org/10.12952/journal.elementa.000017, 2013.

Leck, C. and Persson, C.: Seasonal and short-term variability in dimethyl sulfide, sulfur dioxide and biogenic sulfur and sea salt aerosol particles in the arctic marine boundary layer during summer and autumn, Tellus B, 48(2), 272−299, https://doi.org/10.3402/tellusb.v48i2.15891, 1996.

Lee, K., Sabine, C. L., Tanhua, T., Kim, T. W., Feely, R. A., and Kim, H. C.: Roles of marginal seas in absorbing and storing fossil fuel CO_2, Energ. Environ. Sci., 4(4), 1133−1146, https://doi.org/10.1039/C0EE00663G, 2011.

Lee, H., Park, K.-T., Lee, K., Jeong, H. J., and Yoo, Y. D.: Prey-dependent retention of dimethylsulfoniopropionate (DMSP) by mixotrophic dinoflagellates, Environ. Microbiol., 14, 605–616, https://doi.org/10.1111/j.1462-2920.2011.02600.x, 2012.

Legrand, M., and Pasteur, E. C.: Methane sulfonic acid to non-sea-salt sulfate ratio in coastal Antarctic aerosol and surface snow, J. Geophys. Res.-Atmos., 103(D9), 10991−11006, https://doi.org/10.1029/98JD00929, 1998.

Levasseur, M.: Impact of Arctic meltdown on the microbial cycling of sulphur, Nat. Geosci., 6(9), 691−700, https://doi.org/10.1038/ngeo1910, 2013.

Li, S. M., and Barrie, L. A.: Biogenic sulfur aerosol in the Arctic troposphere: 1. Contributions to total sulfate, J. Geophys. Res.-Atmos., 98(D11), 20613−20622, https://doi.org/10.1029/93JD02234, 1993.

Li, S. M., Barrie, L. A., Talbot, R. W., Harriss, R. C., Davidson, C. I., and Jaffrezo, J. L.: Seasonal and geographic variations of methanesulfonic acid in the Arctic troposphere, Atmos. Environ. A.-Gen., 27(17-18), 3011−3024, https://doi.org/10.1016/0960-1686(93)90333-T, 1993.

Lin, C. T., Baker, A. R., Jickells, T. D., Kelly, S., and Lesworth, T.: An assessment of the significance of sulphate sources over the Atlantic Ocean based on sulphur isotope data, Atmos. Environ., 62, 615–621, https://doi.org/10.1016/j.atmosenv.2012.08.052, 2012.

Mahowald, N., Ward, D., Kloster, S., Flanner, M., Heald, C., Heavens, N., Hess, P., Lamarque, J.-F., and Chuang, P.: Aerosol impacts on climate and biogeochemistry, Annu. Rev. Env. Resour., 36, 45–74, https://doi.org/10.1146/annurev-environ-042009-094507, 2011.

Massling, A., Nielsen, I. E., Kristensen, D., Christensen, J. H., Sørensen, L. L., Jensen, B., Nguyen, Q. T., Nøjgaard, J. K., Glasius, M. and Skov, H.: Atmospheric black carbon and sulfate concentrations in Northeast Greenland, Atmos. Chem. Phys., 15(16), 9681–9692, https://doi.org/10.5194/acp-15-9681-2015, 2015.

Moffett, C. E., Barrett, T. E., Liu, J., Gunsch, M. J., Upchurch, L. M., Quinn, P. K., Pratt, K. A., and Sheesley, R. J.: Long-Term Trends for Marine Sulfur Aerosol in the Alaskan Arctic and Relationships With Temperature, J. Geophys. Res.-Atmos., 125(22), e2020JD033225, https://doi.org/10.1029/2020JD033225, 2020.

Mungall, E. L., Croft, B., Lizotte, M., Thomas, J. L., Murphy, J. G., Levasseur, M., Martin, R. V., Wentzell, J. J. B., and Abbatt, J. P. D.: Dimethyl sulfide in the summertime Arctic atmosphere: measurements and source sensitivity simulations, Atmos. Chem. Phys., 16(11), 6665–6680, https://doi.org/10.5194/acp-16-6665-2016, 2016.

650   Norman, A. L., Barrie, L. A., Toom-Sauntry, D., Sirois, A., Krouse, H. R., Li, S. M., and Sharma, S.: Sources of aerosol sulphate at Alert: Apportionment using stable isotopes, J. Geophys. Res.-Atmos., 104, 11619–11631, https://doi.org/10.1029/1999JD900078, 1999.

Park, K.-T., Lee, K., Yoon, Y.-J., Lee, H.-W., Kim, H.-C., Lee, B.-Y., Hermansen, O., Kim, T.-W., Holmén, K.: Linking atmospheric dimethyl sulfide (DMS) and the Arctic Ocean spring bloom, Geophys. Res. Lett., 40, 155–160,
655   https://doi.org/10.1029/2012GL054560, 2013.

Park, K.-T., Lee, K., Shin, K., Yang, E. J., Hyun, B., Kim, J.-M., Noh, J. H., Kim, M., Kong, B., Choi, D. H., Choi, S.-J., Jang, P.-G., and Jeong, H. J.: Direct linkage between dimethyl sulfide production and microzooplankton grazing, resulting from prey composition change under high partial pressure of carbon dioxide conditions, Environ. Sci. Technol., 48, 4750–4756, https://doi.org/10.1021/es403351h, 2014a.

660   Park, K.-T., Lee, K., Shin, K., Jeong, H. J., and Kim, K. Y.: Improved method for minimizing sulfur loss in analysis of particulate organic sulfur. Anal. Chem., 86(3), 1352–1356. https://doi.org/10.1021/ac403649m, 2014b.

Park, K.-T., Jang, S., Lee, K., Yoon, Y. J., Kim, M.-S., Park, K., Cho, H.-J., Kang, J.-H., Udisti, R., Lee, B.-Y., and Shin, K.-H.: Observational evidence for the formation of DMS-derived aerosols during Arctic phytoplankton blooms, Atmos. Chem. Phys., 17, 9665–9675, https://doi.org/10.5194/acp-17-9665-2017, 2017.

665   Park, K.-T., Lee, K., Kim, T. W., Yoon, Y. J., Jang, E. H., Jang, S., Lee, B.-Y., and Hermansen, O.: Atmospheric DMS in the Arctic Ocean and its relation to phytoplankton biomass, Global. Biogeochem. Cy., 32(3), 351–359, https://doi.org/10.1002/2017GB005805, 2018.

Park, K., Kim, I., Choi, J. O., Lee, Y., Jung, J., Ha, S. Y., Kim, J. H., and Zhang, M.: Unexpectedly high dimethyl sulfide concentration in high-latitude Arctic sea ice melt ponds, Environ. Sci.-Proc. Imp., 21(10), 1642–1649,
670   https://doi.org/10.1039/C9EM00195F, 2019.

Prospero, J. M., Savoie, D. L., Saltzman, E. S., and Larsen, R.: Impact of oceanic sources of biogenic sulphur on sulphate aerosol concentrations at Mawson, Antarctica, Nature, 350(6315), 221−223, https://doi.org/10.1038/350221a0, 1991.

Pszenny, A. A., Castelle, A. J., Galloway, J. N., and Duce, R. A.: A study of the sulfur cycle in the Antarctic marine boundary layer, J. Geophys. Res.-Atmos., 94(D7), 9818−9830, https://doi.org/10.1029/JD094iD07p09818, 1989.

675   Pszenny, A. A.: Particle size distributions of methanesulfonate in the tropical Pacific marine boundary layer, J. Atmos. Chem., 14(1-4), 273−284, https://doi.org/10.1007/BF00115239, 1992.

Read, K. A., Lewis, A. C., Bauguitte, S., Rankin, A. M., Salmon, R. A., Wolff, E. W., Saiz-Lopez, A., Bloss, W. J., Heard, D. E., Lee, J. D., and Plane, J. M. C.: DMS and MSA measurements in the Antarctic Boundary Layer: impact of BrO on MSA production, Atmos. Chem. Phys., 8, https://doi.org/10.5194/acp-8-2985-2008, 2985−2997, 2008.

680   Rinaldi, M., Fuzzi, S., Decesari, S., Marullo, S., Santoleri, R., Provenzale, A., Hardenberg, J., Ceburnis, D., Vaishya, A., O'Dowd, C. D., and Facchini, M. C.: Is chlorophyll-*a* the best surrogate for organic matter enrichment in submicron primary marine aerosol?, J. Geophys. Res.-Atmos., 118, 4964–4973, doi:10.1002/jgrd.50417, 2013.

Sanchez, K. J., Chen, C. L., Russell, L. M., Betha, R., Liu, J., Price, D. J., Massoli, P., Ziemba, L. D., Crosble, E. C., Moore, R. H., Müller, M., Schiller, S. A., Wisthaler, A., Lee, A. K. Y., Quinn P. K., Bates, T. S., Porter, J., Bell, T. G., Saltzman, E. S., Vaillancourt R. D., Behrenfeld, M. J.,: Substantial seasonal contribution of observed biogenic sulfate particles to cloud condensation nuclei, Sci. Rep., 8(1), 1−14, https://doi.org/10.1038/s41598-018-21590-9, 2018.

Santamaria-Fernandez, R., Hearn, R., and Wolff, J. C.: Detection of counterfeit tablets of an antiviral drug using $\delta^{34}S$ measurements by MC-ICP-MS and confirmation by LA-MC-ICP-MS and HPLC-MC-ICP-MS, J. Anal. Atom. Spectrom., 23(9), 1294–1299, https://doi.org/10.1039/B802890G, 2008.

Saltzman, E. S., Savoie, D. L., Prospero, J. M., and Zika, R. G.: Methanesulfonic acid and non-sea-salt sulfate in Pacific air: Regional and seasonal variations, J. Atmos. Chem., 4(2), 227−240, https://doi.org/10.1007/BF00052002, 1986.

Savoie, D. L., Prospero, J. M., Larsen, R. J., and Saltzman, E. S.: Nitrogen and sulfur species in aerosols at Mawson, Antarctica, and their relationship to natural radionuclides, J. Atmos. Chem., 14(1-4), 181–204, https://doi.org/10.1007/BF00115233, 1992.

Sekiguchi, M., Nakajima, T., Suzuki, K., Kawamoto, K., Higurashi, A., Rosenfeld, D., Sano, I., and Mukai, S.: A study of the direct and indirect effects of aerosols using global satellite data sets of aerosol and cloud parameters, J. Geophys. Res., 108, 4699, https://doi.org/10.1029/2002JD003359, https://doi.org/10.1029/2002JD003359, 2003.

Stefels, J., Steinke, M., Turner, S., Malin, G., and Belviso, S.: Environmental constraints on the production and removal of the climatically active gas dimethylsulphide (DMS) and implications for ecosystem modelling, Biogeochemistry, 83, 245–275, https://doi.org/10.1007/s10533-007-9091-5, 2007.

Stroeve, J. C., Jenouvrier, S., Campbell, G. G., Barbraud, C., and Delord, K.: Mapping and assessing variability in the Antarctic marginal ice zone, pack ice and coastal polynyas in two sea ice algorithms with implications on breeding success of snow petrels, The Cryosphere, 10(4), 1823–1843, https://doi.org/10.5194/tc-10-1823-2016, 2016.

Udisti, R., Dayan, U., Becagli, S., Busetto, M., Frosini, D., Legrand, M., Lucarelli, F., Preunkert, S., Severi, M., Traversi, R., and Vitale, V.: Sea spray aerosol in central Antarctica. Present atmospheric behaviour and implications for paleoclimatic reconstructions, Atmos. Environ., 52, 109–120, 2012.

Udisti, R., Bazzano, A., Becagli, S., Bolzacchini, E., Caiazzo, L., Cappelletti, D., Ferrero, L., Frosini, D., Giardi, F., Grotti, M., Lupi, A., Malandrino, M., Mazzola, M., Moroni, B., Severi, M., Traversi, R., Viola, A., and Vitale, V.: Sulfate source apportionment in the Ny Ålesund (Svalbard Islands) Arctic aerosol, Rend. Lincei, 27, S85–S94, https://doi.org/10.1007/s12210-016-0517-7, 2016.

Vallina, S. M., Simó, R., and Gassó, S.: What controls CCN seasonality in the Southern Ocean? A statistical analysis based on satellite-derived chlorophyll and CCN and model-estimated OH radical and rainfall, Global. Biogeochem. Cy., 20(1), GB1014, https://doi.org/10.1029/2005GB002597, 2006.

Vallina, S. M., Simó, R., Gassó, S., de Boyer-Montégut, C., Del Río, E., Jurado, E., and Dachs, J.: Analysis of a potential "solar radiation dose–dimethylsulfide–cloud condensation nuclei" link from globally mapped seasonal correlations, Global. Biogeochem. Cy., 21(2), GB2004, https://doi.org/10.1029/2006GB002787, 2007.

Veres, P. R., Neuman, J. A., Bertram, T. H., Assaf, E., Wolfe, G. M., Williamson, C. J., Weinzierl, B., Tilmes, S., Thompson, C. R., Thames, A. B., Schroder, J. C., Saiz-Lopez, A., Rollins, A. W., Roberts, J. M., Price, D., Peischl, J., Nault, B. A., Møller, K. H., Miller, D. O., Meinardi, S., Li, Q., Lamarque, J., Kupc, A., Kjaergaard, H. G., Kinnison, D., Jimenez, J. L., Jernigan, C. M., Hornbrook, R. S., Hills, A., Dollner, M., Day, D. A., Cuevas, C. A., Campuzano-Jost, P., Burkholder, J., Bui, T. P., Brune, W. H., Brown, S. S., Brock, C. A., Bourgeois, I., Black, D. R., Apel, E. C., and Ryerson, T. B.,: Global airborne sampling reveals a previously unobserved dimethyl sulfide oxidation mechanism in the marine atmosphere, P. Natl. Acad. Sci. USA, 117(9), 4505–4510, https://doi.org/10.1073/pnas.1919344117, 2020.

von Glasow, R., and Crutzen, P. J.: Model study of multiphase DMS oxidation with a focus on halogens, Atmos. Chem. Phys., 4, 589–608, https://doi.org/10.5194/acp-4-589-2004, 2004.

Willis, M. D., Leaitch, W. R., and Abbatt, J. P.: Processes controlling the composition and abundance of Arctic aerosol, Rev. Geophys., 56(4), 621−671, https://doi.org/10.1029/2018RG000602, 2018.

Wyslouzil, B. E., Seinfeld, J. H., Flagan, R. C., and Okuyama, K.: Binary nucleation in acid–water systems. I. Methanesulfonic acid–water, J. Chem. Phys., 94(10), 6827−6841, https://doi.org/10.1063/1.460261, 1991.

Yan, J., Zhang, M., Jung, J., Lin, Q., Zhao, S., Xu, S., and Chen, L.: Influence on the conversion of DMS to MSA and SO_4^{2-} in the Southern Ocean, Antarctica, Atmos. Environ., 117611, https://doi.org/10.1016/j.atmosenv.2020.117611, 2020a.

Yan, J., Jung, J., Zhang, M., Bianchi, F., Tham, Y. J., Xu, S., Lin, Q., Zhao, S., Li, L., and Chen, L.: Uptake selectivity of methanesulfonic acid (MSA) on fine particles over polynya regions of the Ross Sea, Antarctica, Atmos. Chem. Phys., 20, 3259−3271, https://doi.org/10.5194/acp-20-3259-2020, 2020b.

Yin, F., Grosjean, D., and Seinfeld, J. H.: Photooxidation of dimethyl sulfide and dimethyl disulfide. I: Mechanism development, J. Atmos. Chem., 11(4), 309−364, https://doi.org/10.1007/BF00053780, 1990.

Zhan, J., Li, W., Chen, L., Lin, Q., and Gao, Y.: Anthropogenic influences on aerosols at Ny-Ålesund in the summer Arctic, Atmos. Pollut. Res., 8(2), 383–393, https://doi.org/10.1016/j.apr.2016.10.010, 2017.
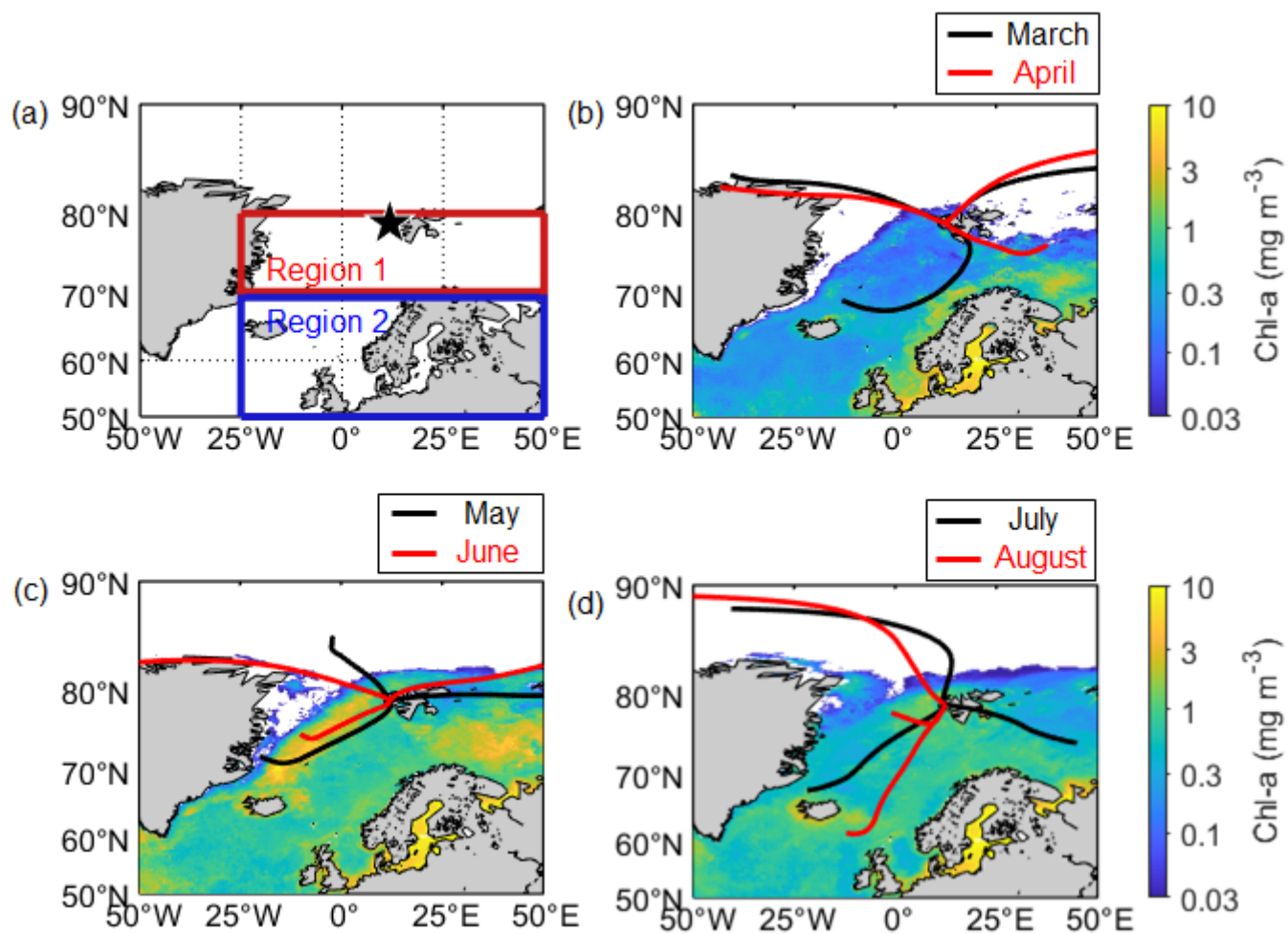
Figure 1: (a) Location of the aerosol sampling site (black pentagram; Gruvebadet observatory; 78.9° N, 11.9° E) and the ocean domains (70° N–80° N, 25° W–50° E for Region 1; 50° N–70° N, 25° W–50° E for Region 2) defined for this study. Mean Chl-*a* concentration for (b) March and April, (c) May and June, and (d) July and August over the period of 2015–2019, overlaid with air mass trajectory clusters that represent the dominant pathways of air masses reaching to the observation site.
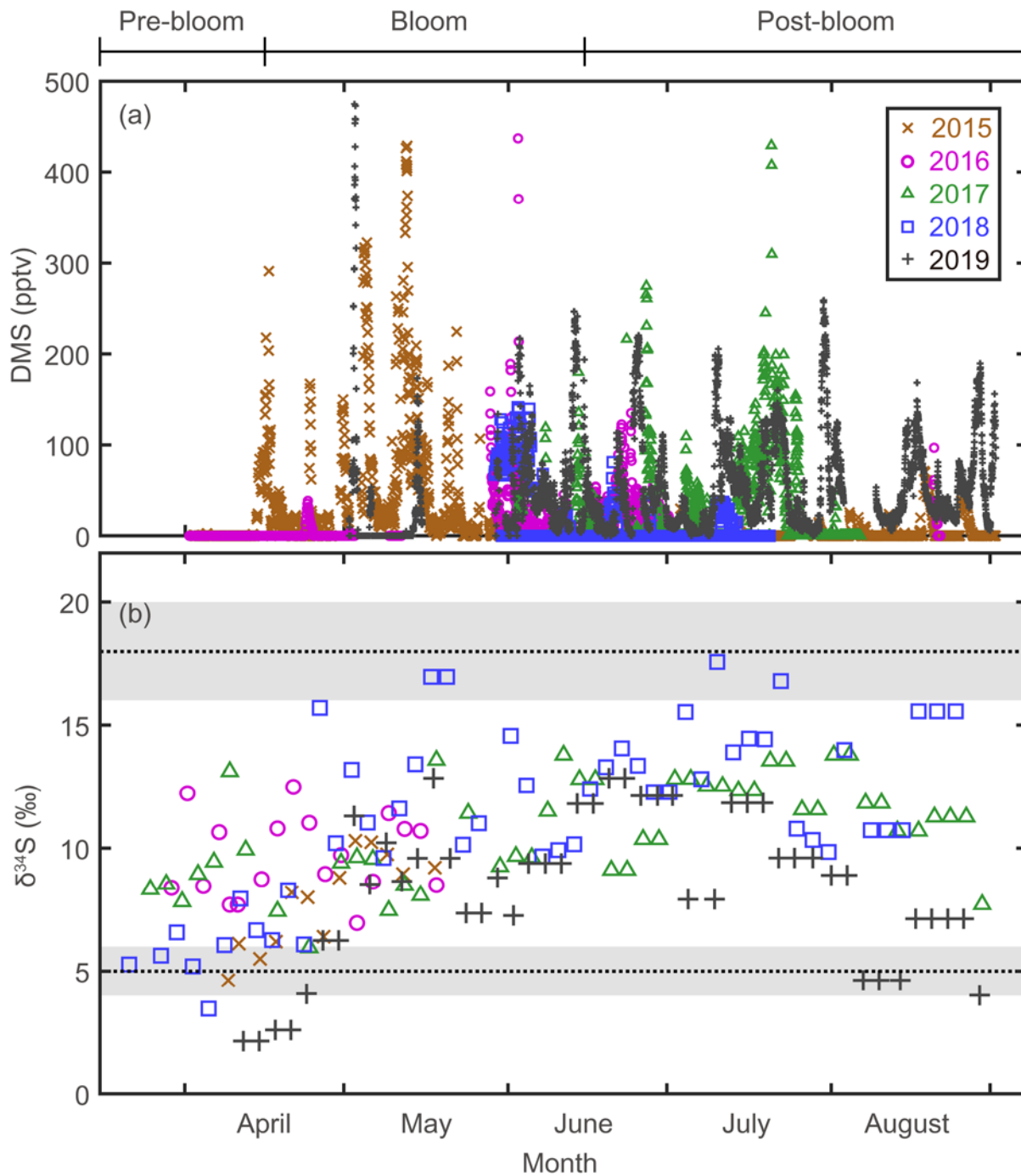
Figure 2: (a) Atmospheric DMS mixing ratios measured at Zeppelin station, Svalbard, in 2015, 2016, 2017, 2018, and 2019. (b) Stable isotope composition of sulfate aerosols. Three end-member values; $\delta^{34}S_{SS} = 21 \pm 0.1$ ‰ for sea-salt sulfates; $\delta^{34}S_{Anth} = 5 \pm 1$ ‰ for anthropogenic sulfate; and $\delta^{34}S_{Bio} = 18 \pm 2$ ‰ for biogenic sulfates.

745
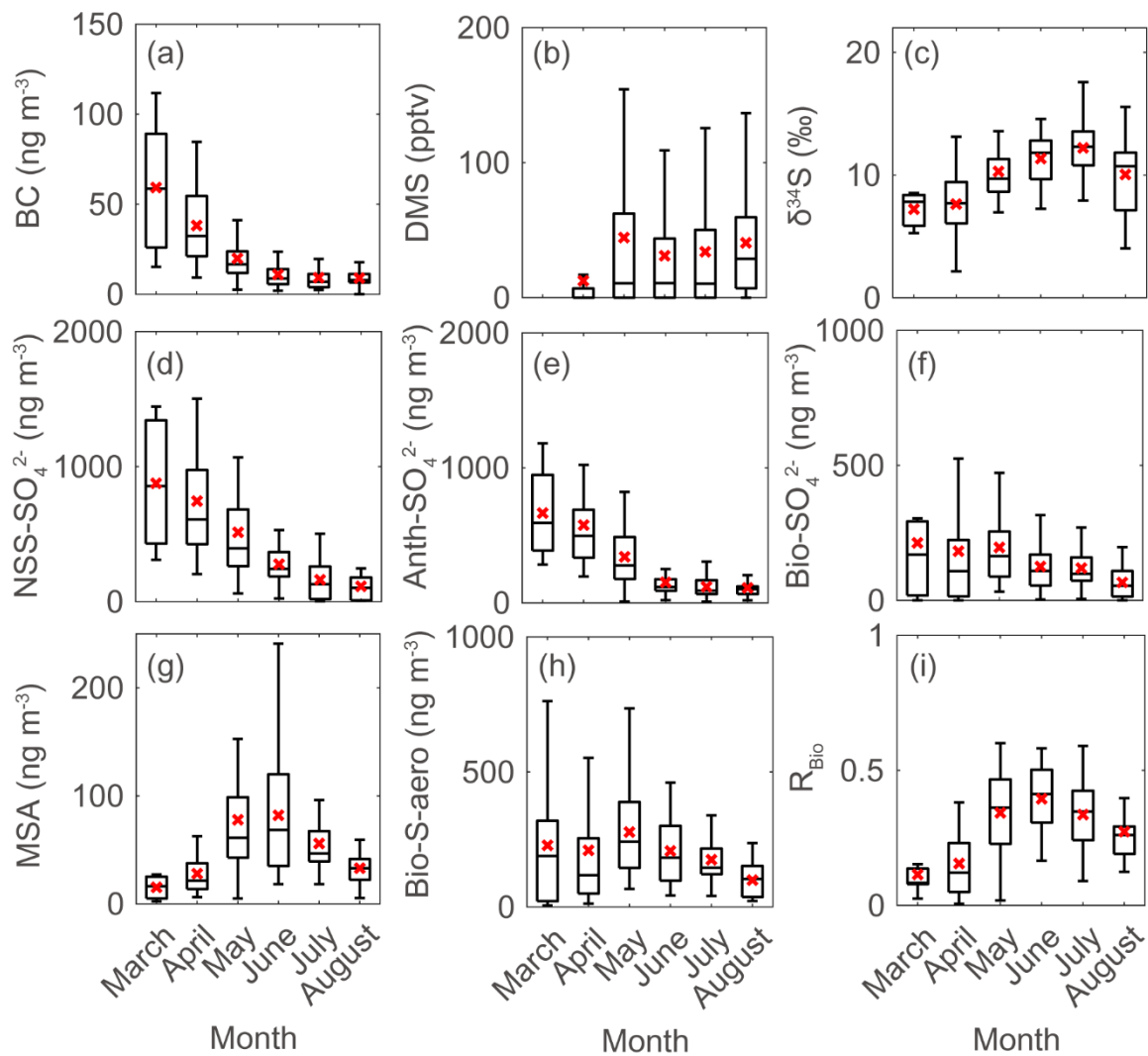
Figure 3: Monthly data during the measurement years (2015-2019) for: (a) black carbon (BC), (b) atmospheric DMS mixing ratio, (c) sulfur isotope measurements (δ^{34}S), (d) NSS-SO$_4^{2-}$, (e) Anth-SO$_4^{2-}$, (f) Bio-SO$_4^{2-}$, (g) MSA, (h) Bio-S-aerosol, and (i) MSA to Bio-S-aerosol ratio (R$_{Bio}$) during the measurement years (2015–2019). Solid lines and red crosses represent the median and mean values of the data, respectively.
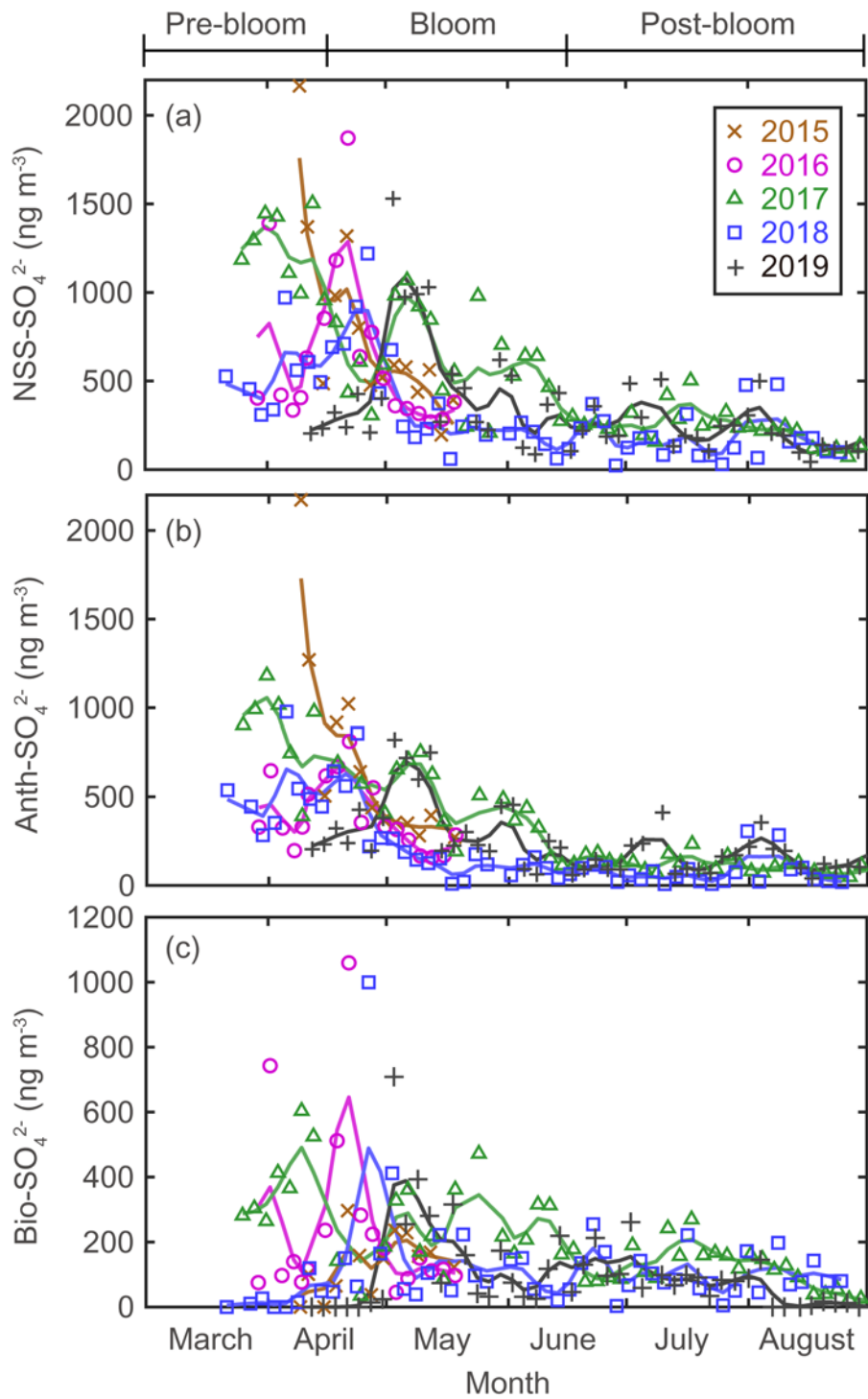
Figure 4: Aerosol concentrations for: (a) NSS-SO$_4^{2-}$ (total SO$_4^{2-}$ minus ss-SO$_4^{2-}$); (b) Anth-SO$_4^{2-}$, and (c) Bio-SO$_4^{2-}$. The colored solid lines indicate 15-day moving average values.
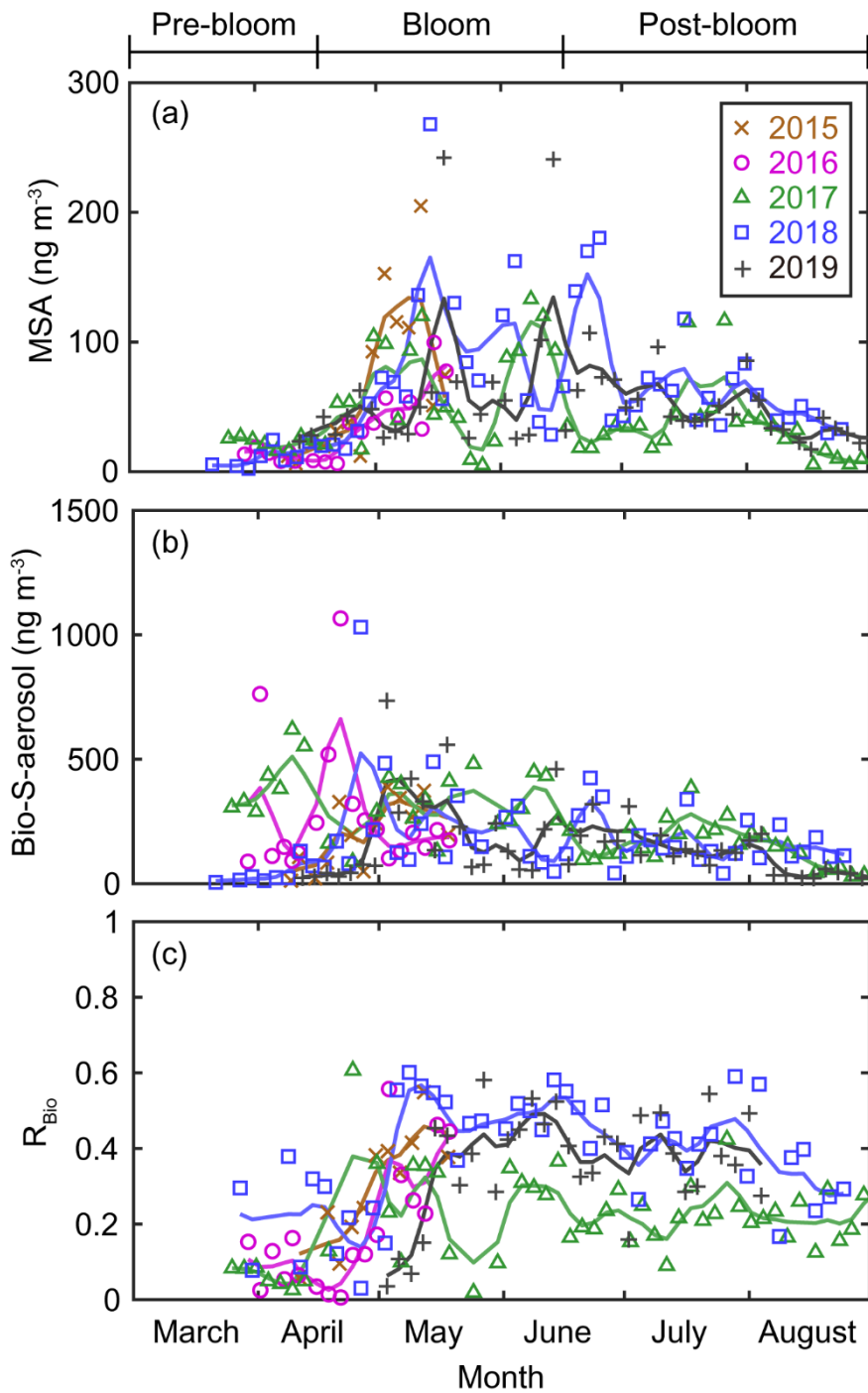
Figure 5: Aerosol concentrations of (a) MSA and (b) Bio-S-aerosol (MSA + Bio-SO$_4^{2-}$). (c) Variations in the ratio of MSA to Bio-S-aerosol (R$_{Bio}$). The colored solid lines indicate 15-day moving mean values.

750
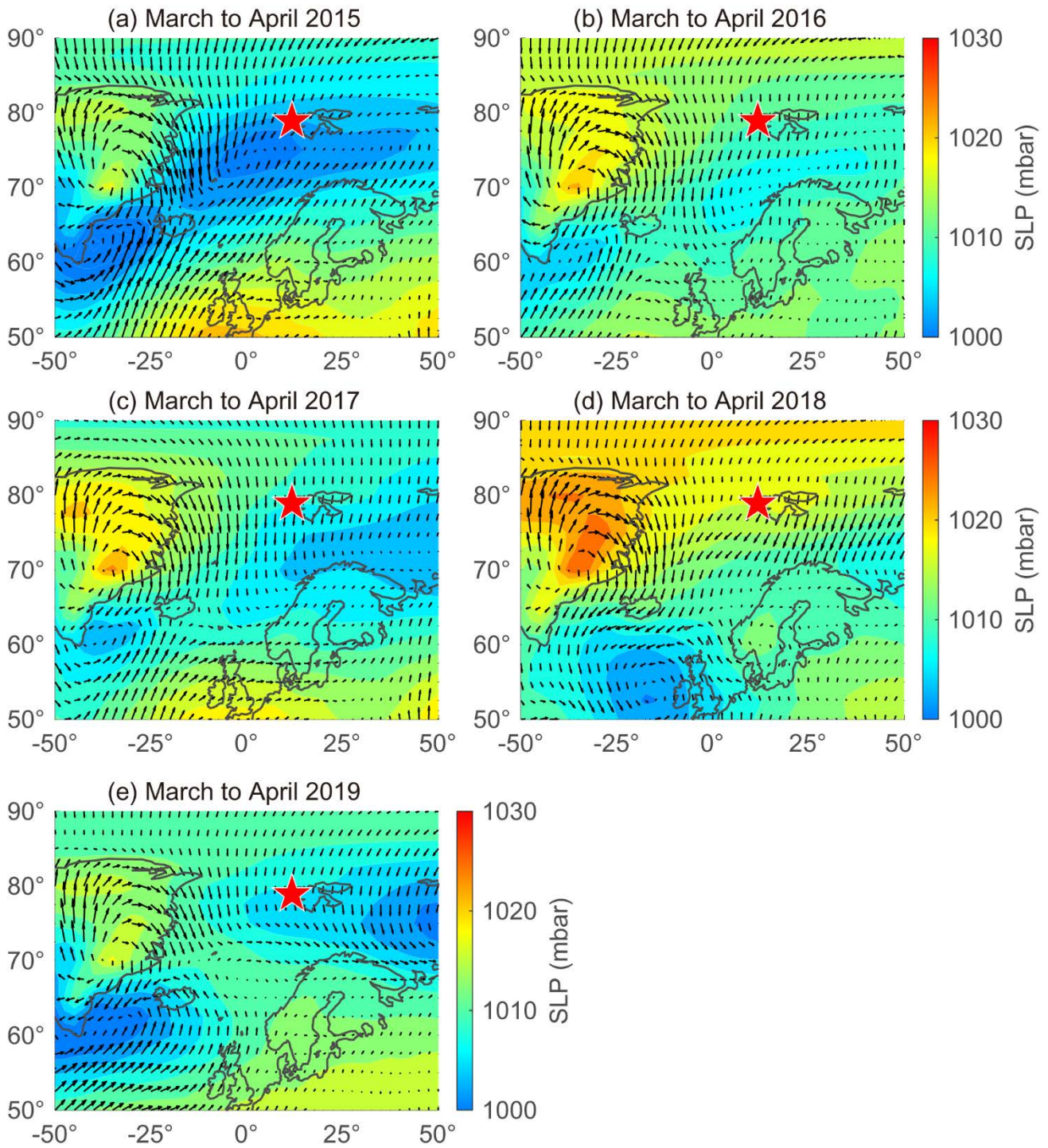
Figure 6: Sea level pressure (SLP) overlaid with wind vectors during March to April in (a) 2015, (b) 2016, (c) 2017, (d) 2018, and (b) 2019. Red stars indicate the location of the sampling site (Gruvebadet observatory; 78.9° N, 11.9° E).
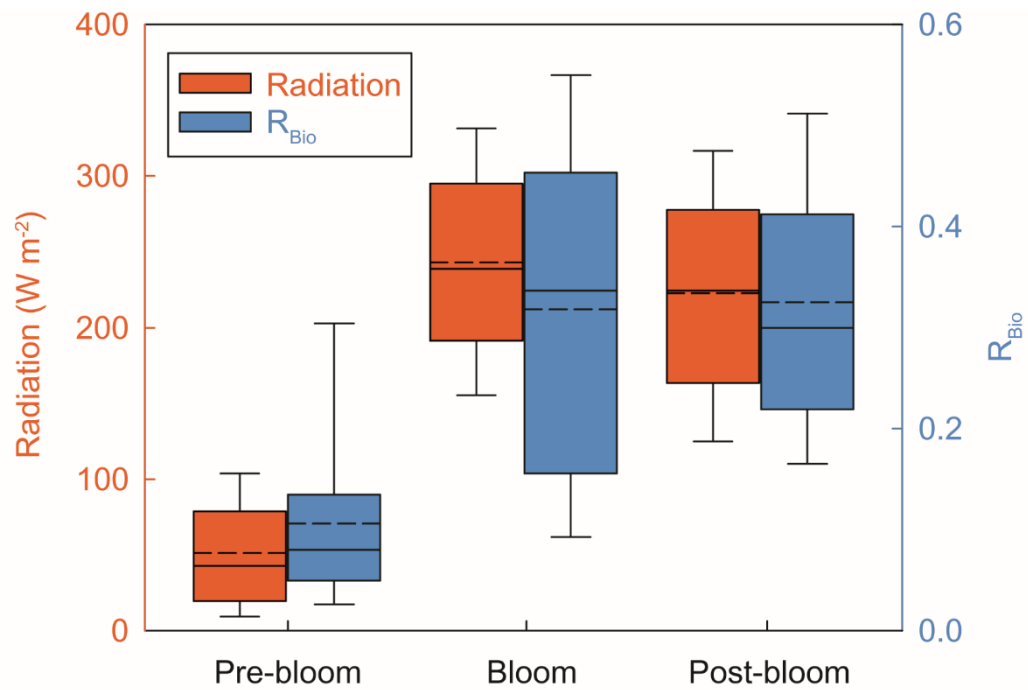
Figure 7: Five-year (2015, 2016, 2017, 2018 and 2019) mean radiation (red) and R_{Bio} (blue) during the pre-bloom, bloom, and post-bloom periods. Solid line and dotted line represent median and mean value of each data in box plot, respectively.
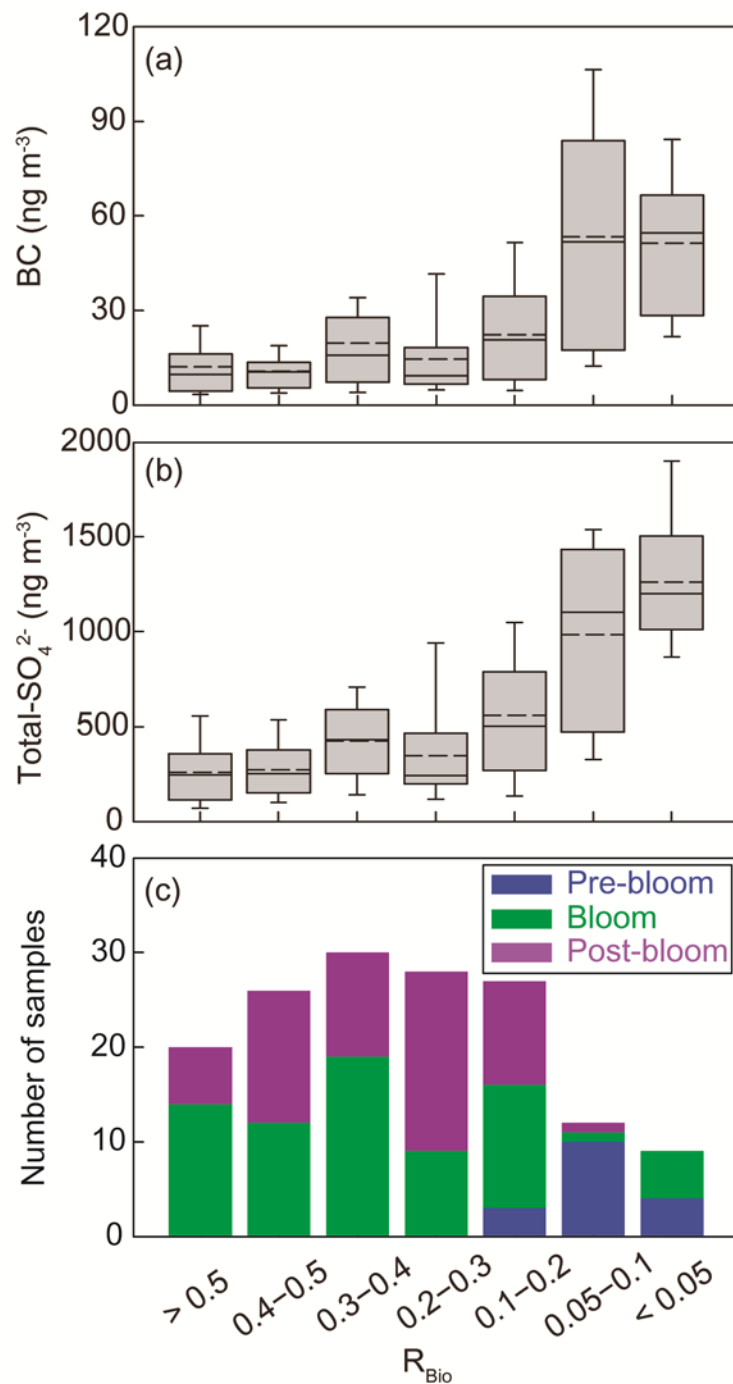
Figure 8: Plots of the seasonal (a) black carbon (BC) concentration versus R_{Bio}, (b) the total SO_4^{2-} concentration versus R_{Bio}, and (c) the number of samples included in each R_{Bio} group. The solid and dotted lines represent the median and mean values of the data in the box plots, respectively.
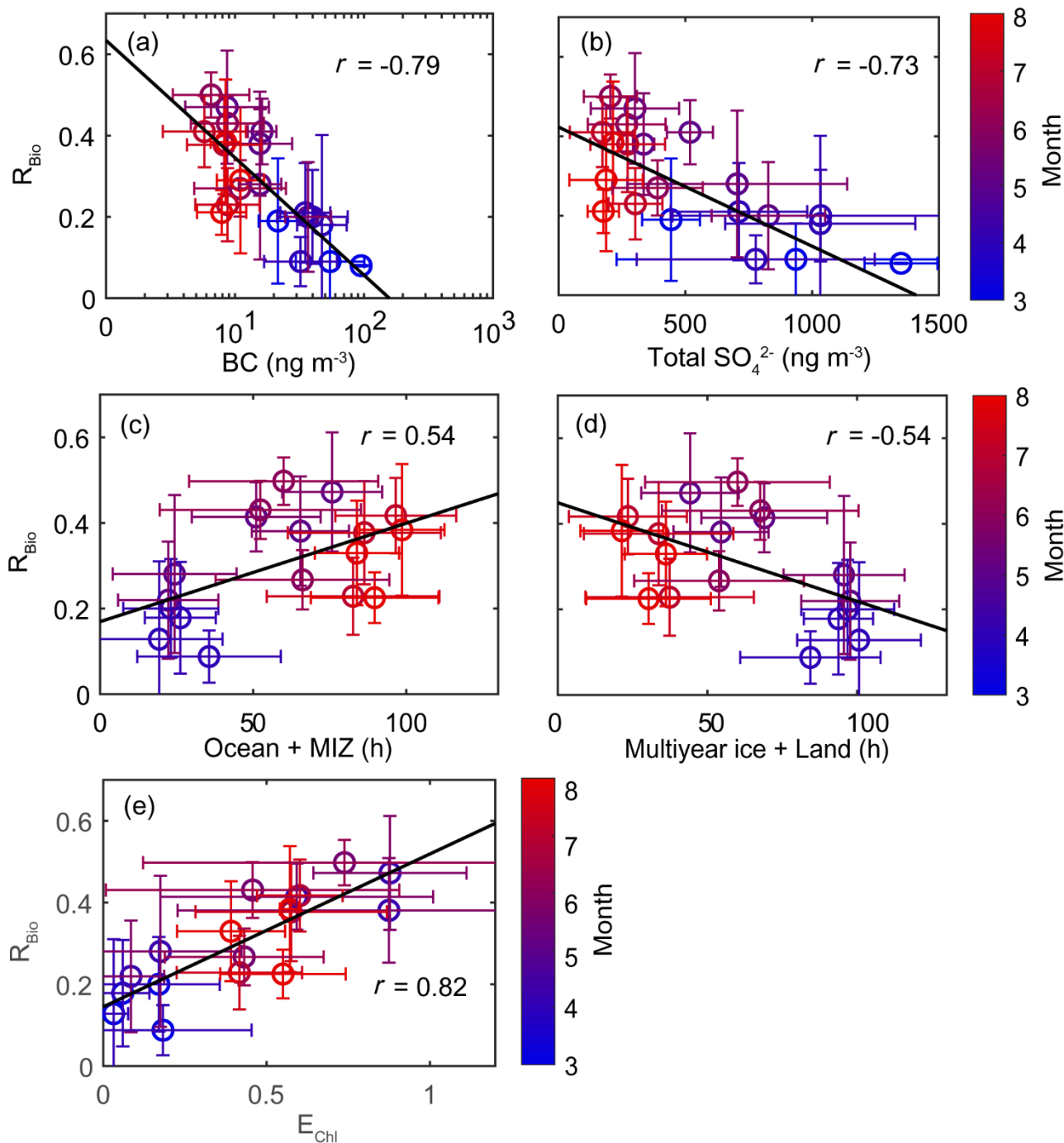
755   Figure 9: Scatter plots of monthly mean R_{Bio} values as a function of: (a) the monthly mean black carbon (BC) concentration; (b) the monthly mean total SO_4^{2-} concentration; (c) the air mass retention time over the ocean and the marginal ice zone (MIZ); (d) the air mass retention time over multi-year ice and land areas; and (e) the monthly mean air mass exposure to chlorophyll (E_{Chl}). Error bars and the black solid line represent 1σ and the best fit, respectively.
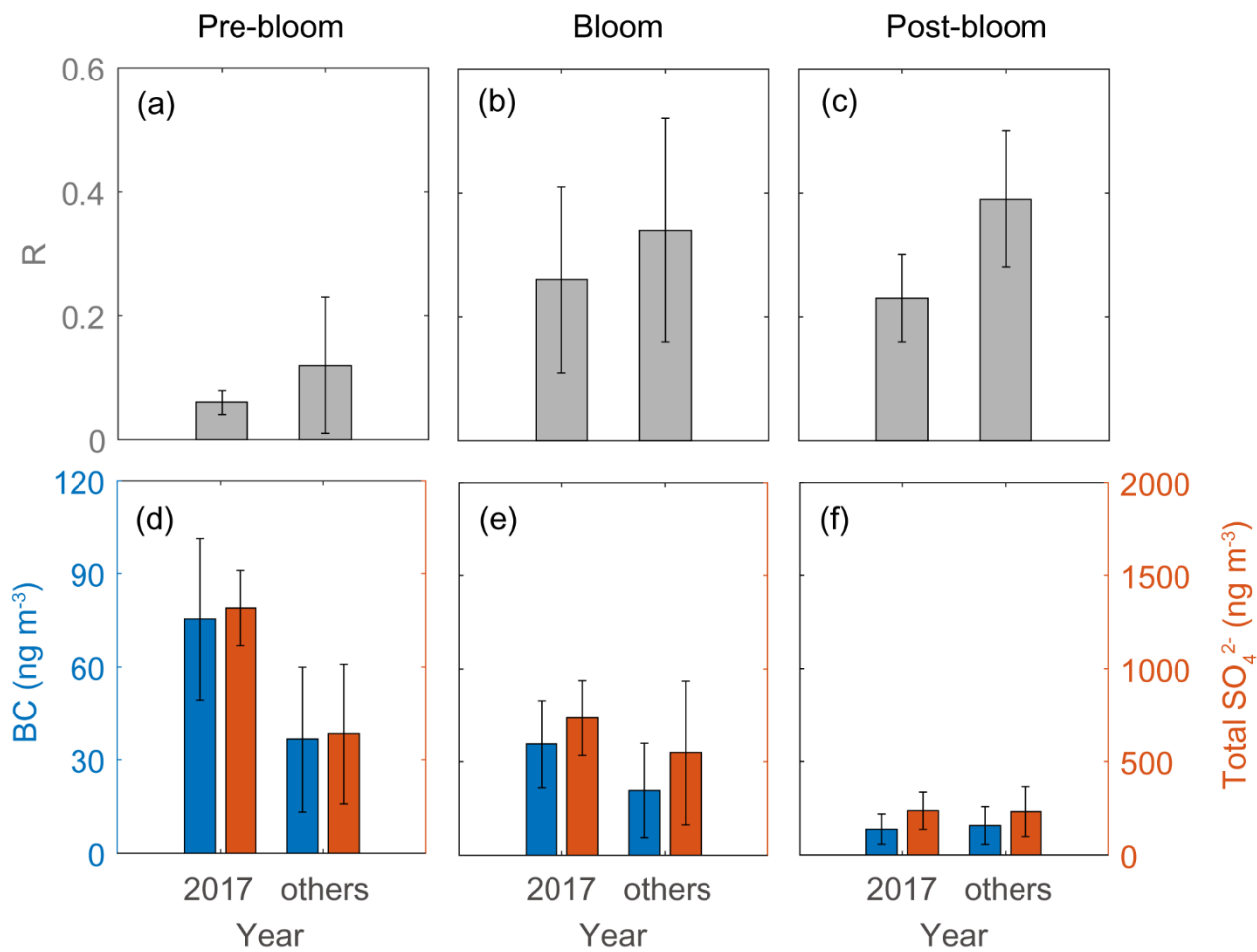
Figure 10: R_{Bio} (a–c) and the black carbon (BC) and total SO_4^{2-} concentrations (d–f) during pre-bloom, bloom, and post-bloom periods. Error bars represent 1σ.
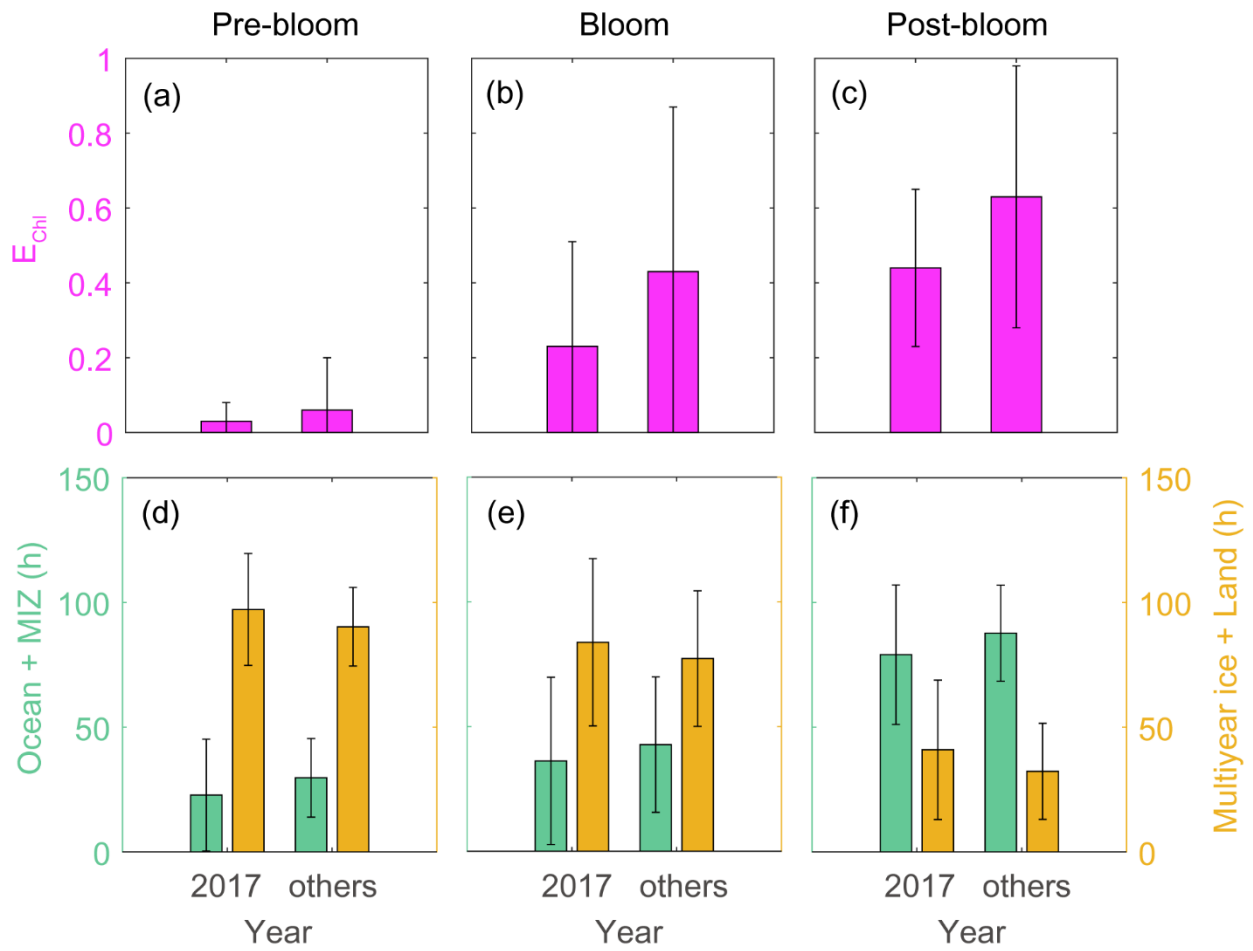
760   Figure 11: Air mass exposure to chlorophyll (E_{Chl}) (a–c) and the air mass residence times over the ocean and marginal ice zone (MIZ) and the multi-year ice and land areas (d–f) during pre-bloom, bloom, post-bloom periods. Error bars represent 1σ.